TUDelft

Delft University of Technology

Programming the shape-shifting of flat soft matter

van Manen, Teunis; Janbaz, Shahram; Zadpoor, Amir A.

Important note
To cite this publication, please use the final published version (if applicable).
Please check the document version above.

Programming the shape-shifting of flat soft matter

Teunis van Manen, Shahram Janbaz *, **Amir A. Zadpoor**

Additive Manufacturing Laboratory, Department of Biomechanical Engineering, Delft University of Technology (TU Delft), Mekelweg 2, Delft 2628CD, The Netherlands

Shape-shifting of flat materials into the desired 3D configuration is an alternative design route for fabrication of complex 3D shapes, which provides many benefits such as access to the flat material surface and the ability to produce well-described motions. The advanced production techniques that primarily work in 2D could then be used to add complex surface features to the flat material. The combination of complex 3D shapes and surface-related functionalities has a wide range of applications in biotechnology, actuators/sensors, and engineering of complex metamaterials. Here, we categorize the different programming strategies that could be used for planning the shape-shifting of soft matter based on the type of stresses generated inside the flat material and present an overview of the ways those mechanisms could be used to achieve the desired 3D shapes. Stress gradients through the thickness of the material, which generate out-of-plane bending moments, and compressive in-plane stresses that result in out-of-plane buckling constitute the major mechanisms through which shape-shifting of the flat matter could be programmed. We review both programming strategies with a focus on the underlying physical principles, which are highly scalable and could be applied to other structures and materials. The techniques used for programming the time sequence of shape-shifting are discussed as well. Such types of so-called "sequential" shape-shifting enable achieving more complex 3D shapes, as the kinematics of the movements could be planned in time to avoid collisions. Ultimately, we discuss what 3D shapes could be achieved through shape-shifting from flat soft matter and identify multiple areas of application.

Introduction

Shape-shifting of initially flat materials into programmed 3D configurations is an emerging area of research that holds a lot of promise for development of complex materials with unprecedented functionalities and properties. A wide range of shape-shifting phenomena are seen in nature and often originate from the spatial arrangement of the structural elements and their differential responses to the different types of stimuli. For example, dimensional transformation of active elements in response to external stimuli could activate the process of change in the shape of materials such as what pine cone [1,2] and Mimosa Pudica [3]

show via the evolution in their extracellular systems. Inspired by nature, synthetic materials have been developed that show highly complex shape transformations once triggered by certain stimuli. Combined with surface-induced functionalities, shape-shifting materials could present functionalities that are unique and relevant for multiple areas of application.

Shape-shifting in synthetic materials may be based on different physical principles such as capillary forces, residual stresses, or the energy released from active polymers [4]. Such active materials may respond to stimuli such as light [5,6], humidity [7], temperature [8], or pH [9], among others. Three main classes of stimuli-responsive polymers have been used in shape-shifting materials [10] and will be shortly introduced here. First, the

* Corresponding author: Janbaz, S. (s.janbaz@tudelft.nl).

swelling/de-swelling of polymer gels has been widely used as a driving force for changing the shape of materials. In response to different stimuli such as temperature or pH, the water uptake inside the crosslinked network could be changed, resulting in reversible volumetric expansion or shrinkage [10,11]. Large swelling ratios up to four orders of magnitude could be obtained, although a large swelling ratio is often linked to a reduced stiffness [12]. However, most hydrogels have limited mechanical properties (i.e. $E < 0.5$ MPa) [13], while the response time is long as compared to other active materials (i.e. up to several hours for material thickness of 1 mm) [14]. Many swellable polymers have good biocompatibility as well as biodegradability, which make them suitable materials for biomedical applications [15,16]. The second class of active polymers are liquid crystalline elastomers (LCE). LCE materials are composed of a liquid crystalline material aligned inside a polymeric network [17,18]. Because of the anisotropic alignment of those molecules, the material stiffness along the alignment direction is larger than those along other directions. Upon activation by different stimuli such as temperature or humidity, the material alignment order will decrease, resulting in highly anisotropic dimensional changes. In contrast to most swellable polymers, the response time of LCE is much shorter [18]. A third widely reported class of active materials are shape memory polymers (SMP), which exhibit the ability to store a temporary shape inside the structure of the material [19,20]. By increasing the temperature above glass transition temperature, Tg, the material softens and can easily be deformed. After reducing the temperature below Tg, this temporary shape will be stored as memory inside the material. Upon activation by different stimuli such as high temperature or light, the relaxation of the polymer results in recovery of the permanent shape. SMP materials exhibits good mechanical properties, although the material stiffness drops dramatically at high temperatures [21]. The main drawback of using SMP as active material is that the dimensional changes are irreversible. Moreover, the material response has to be first programmed inside the material. For a more comprehensive and in-depth review of the structure and functionalities of those and other stimuli responsive materials, the interested reader is referred to other excellent review papers [11,18,19]. In this paper, we review the strategies that could be used to program the shape-shifting of flat soft matter into complex 3D shapes driven by the mechanical forces induced in those active materials. Since many of the presented strategies are based on general physical principles, they could be applied regardless of the type of polymeric materials and the stimulus. Readers interested in the underlying molecular mechanisms or shape-shifting in the broader context of formation of 3D constructs are referred to other recently published reviews [4,14,22]. Here, we focus on the different deformation mechanisms of shape-shifting of flat soft matter from a mechanical point of view, which could serve as a guide for the rational design of shape-shifting materials.

Let us consider a slender (i.e. small thickness as compared to other dimensions) elastic body incorporating a number of active and passive elements. The deformation of such a body could be approximated using the Kirchhoff–Love assumptions [23,24]. In this approach, the deformation of the slender body is represented by the deformation of the mid-plane consisting of the

changes in the planer dimensions and curvature. The elastic energy of the plate could therefore be written as the sum of a stretching term and a bending-related term. Once triggered by the activation stimulus, both bending moments and axial forces may be generated, respectively inducing out-of-plane bending (Fig. 1a) and out-of-plane buckling (Fig. 1b). Creating those two types of forces are the main working principles on which the programming strategies are usually based. Both out-of-plane bending moments and axial (compressive) forces could create the out-of-plane deformations that are required for transforming the shape of a flat material to complex 3D shapes.

It is obvious why an out-of-plane bending moment will cause out-of-plane deformation. The required bending moment is often generated by inducing a gradient in the planar stresses along the thickness of the material upon activation. Different strategies may be used to program such a material response to an activation stimulus (Fig. 1a). In the following section of the paper, we have categorized the reported strategies into three major categories.

As for the (compressive) axial forces, the material will first exhibit a pure stretching state upon activation. Since stretching energy scales linearly with the material thickness while the bending energy has a cubic dependency on the thickness, a bending configuration is energetically favorable over pure stretching for thin constructs [25]. Compressive stresses above a certain critical value will therefore induce out-of-plane buckling of the flat structure, thereby minimizing the elastic energy (Fig. 1b). Different techniques to program the generation of compressive stresses will be reviewed in the third section of the paper.

We will discuss both types of the programming strategies with a focus on the mechanics of deformation and the parameters used to program and control the deformations. In addition to the final shape, the material could be programmed to undergo a specified sequence of deformations over time, thereby achieving more complex shapes. That type of so-called "sequential" shape-shifting will be discussed in the fourth section of this paper.

Bending strategy

As previously stated, a stress gradient along the thickness of the material is required for generating the bending moment. Various approaches comprising different stimuli-responsive materials have been used in the literature for creating the stress gradient, which will be discussed in this section.

Multilayer

A widely applied strategy for generating the bending moments is to combine two layers of different materials into a bilayer construct (Fig. 1a). The swelling/shrinkage mismatch between both layers in response to activation stimuli, while sustaining the same strain at the interface between both layers, could result in different types of deformation. Dependent on the layer thicknesses and the induced strain, both surface wrinkling or bending may be programmed [26]. For example, surface wrinkling may be generated due to the compressive stresses applied on a thin stiff top layer by a thick soft substrate, while global bending could arise in bilayers with comparable stiffness and layer thickness. Here, only out-of-plane bending will be considered. Upon activation, the deformation of the main straining layer is
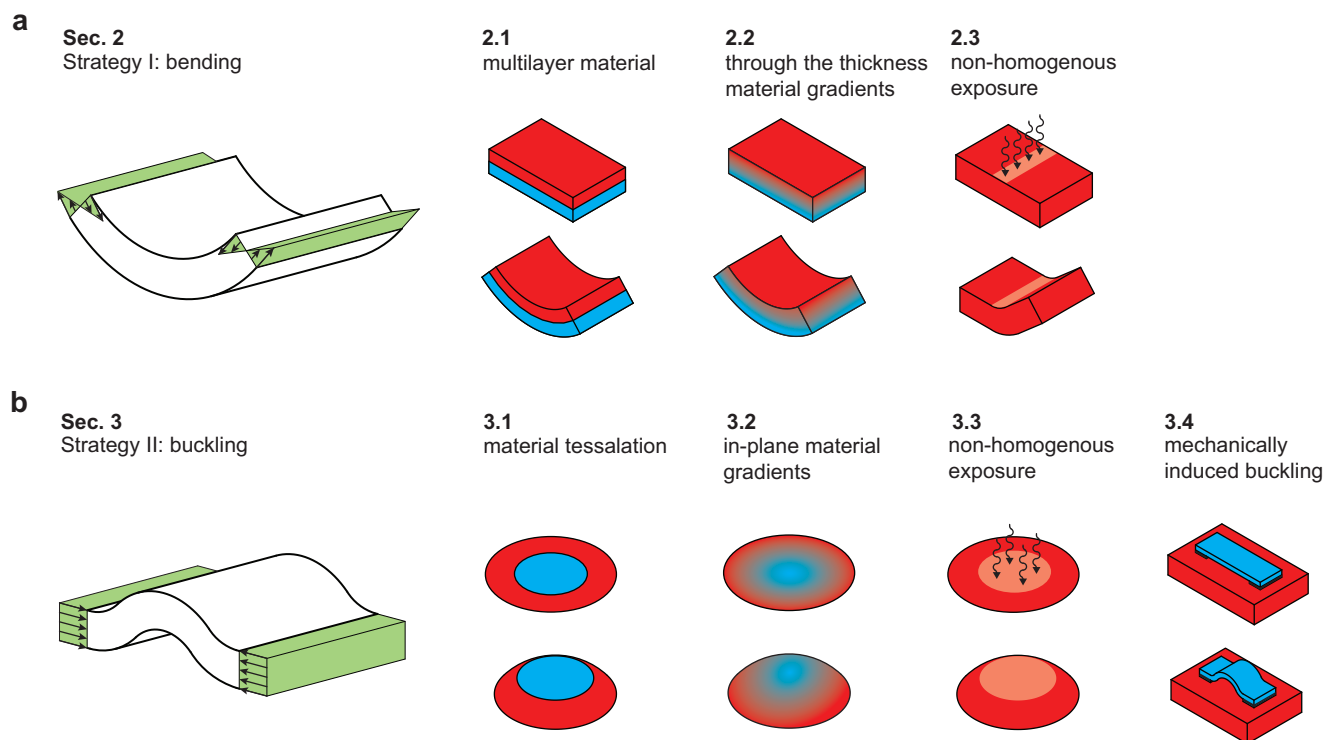
a

Sec. 2
Strategy I: bending

2.1
multilayer material

2.2
through the thickness material gradients

2.3
non-homogenous exposure

b

Sec. 3
Strategy II: buckling

3.1
material tessalation

3.2
in-plane material gradients

3.3
non-homogenous exposure

3.4
mechanically induced buckling

FIGURE 1

Two different strategies for programming 2D/3D shape-shifting. (a) By generating a stress gradient along the thickness of the material, a bending moment may be generated resulting in out-of-plane bending. The different approaches have been divided into three sub-categories. (b) Compressive stresses may induce out-of-plane buckling. Four different categories have been identified within the buckling strategy.

constrained by the second layer and therefor one layer is loaded in tension while compressive stresses are observed in the other layer. The generated bending moment results in global bending of the constructs, thereby (partially) releasing those internal stresses. The general theory of bilayers, developed by Timoshenko [27], states that a bilayer made of two materials with different thermal expansion coefficients result in a uniform curvature, which is inversely proportional to the thickness. The normalized curvature $\tilde{\kappa}$ can be expressed as

$$\tilde{\kappa} = \frac{\kappa h}{\Delta \alpha} = \frac{6(1+m)^2}{3(1+m)^2 + (1+mn)(m^2 + \frac{1}{mn})}$$

where κ is bilayer curvature, h is thickness, $\Delta \alpha$ is the mismatch in the thermal expansion coefficients, n is the stiffness ratio of both layers and m is the thickness ratio of both layers. Fig. 2a depicts the dependency of the normalized bilayer curvature on the thickness ratio of layers and material stiffness ratio. A maximum value of 1.5 is found for the normalized curvature. Although this theory is derived for bi-metallic strips with small thicknesses (i.e. $h \ll L$), its general concept is applicable also to predict the behavior of polymeric materials with different activation mechanisms [22]. In this section, we will discuss structures comprising multiple isotropic material layers as well as multilayer constructs with anisotropic material properties.

Isotropic multilayers

Isotropic swelling/de-swelling of polymers has been reported in many studies as the activation mechanism to drive the bending of bilayer constructs [28–38]. Guan et al. fabricated slender bilayer strips ($95 \times 20 \times 4.8 \, \mu m$) from hydrogels with different amounts of swelling using a soft lithography production process [30]. The curvature of the bilayer strip could be controlled based on the swelling ratios, which originate from different polymer compositions. Keeping the thickness ratio between the active and passive layers around 15, a reduction in the radius of curvature from 80 µm to 30 µm could be achieved based on an increase in the swelling ratio from 15% to 42%. Due to the increase in the swelling ratio, a larger bending moment could be generated, resulting in a larger curvature. More complex 3D microstructures could be made by different combinations of bilayers strips (Fig. 2b). The effects of layer thickness on the radius of curvature is experimentally studied by Egunov et al. by varying the thickness ratio between 1/3 and 4, while keeping the thickness of the passive layer constant around 0.32 mm [29]. As the bending stiffness has a cubic dependency on the thickness, while the generated bending moment increases only quadratically with the thickness, the bilayer curvature reduces as the thickness increases. For thickness ratios close to 1, the results were in good agreement with the Timoshenko's bilayer theory and a normalized curvature of about 1.5 was achieved. In accordance to the results of Guan et al. and the general theory of bilayers, a linear relationship between the radius of curvature and swelling ratio is found [29,30]. The other parameter influencing the radius of curvature is the material stiffness ratio, as it adjusts the resistance of the bilayer against deformation [39]. It is important to realize that swelling may strongly affect the stiffness of the active layer.
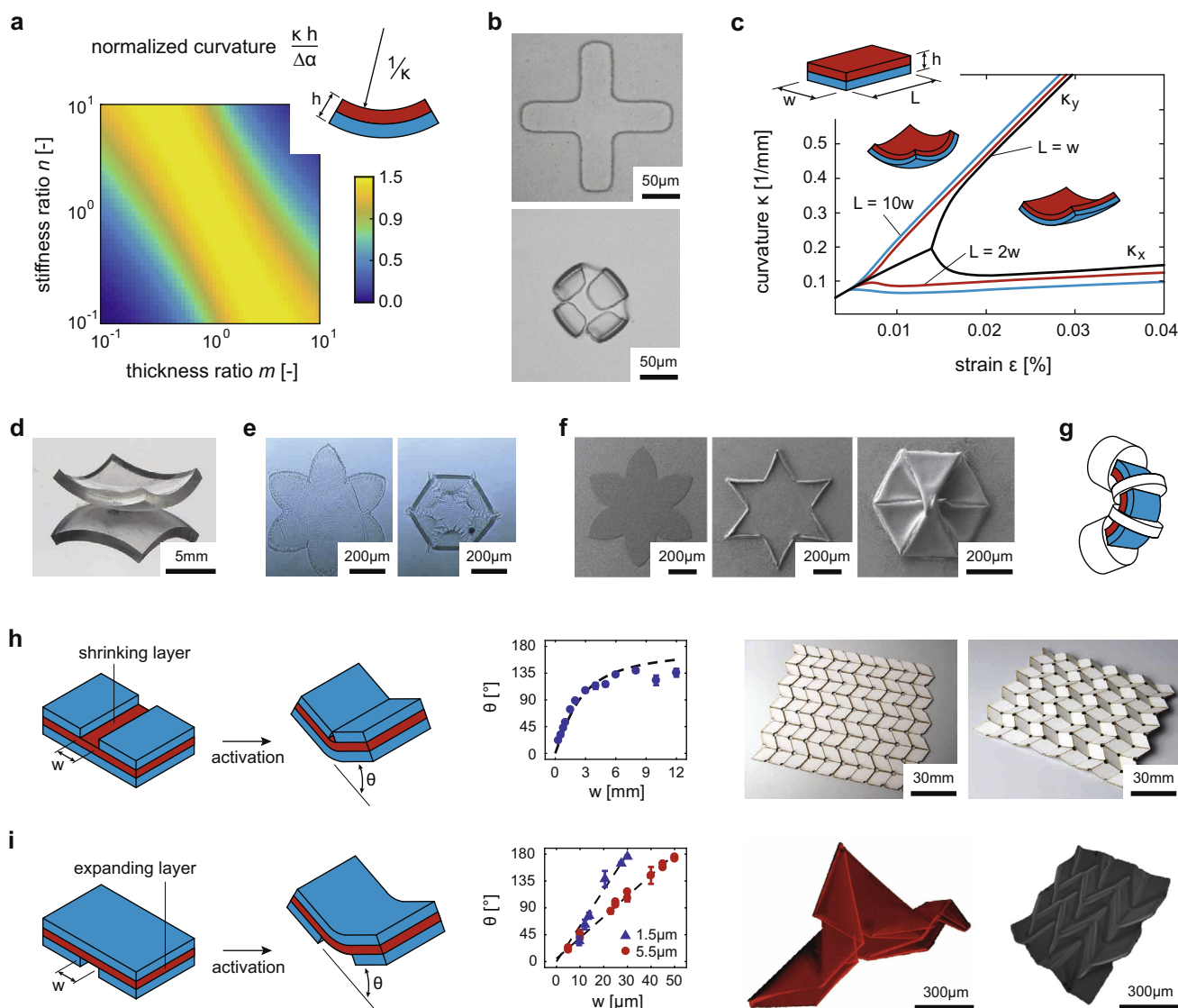
FIGURE 2

(a) The normalized curvature of bilayer samples according to the Timoshenko's theory. (b) Shape-shifting of a cross-shaped bilayer into a 3D constructs. Reproduced with permission from [30]. Copyright 2005 by the American Chemical Society. (c) The two principal curvatures of rectangular isotropic bilayer samples as a function of the strain mismatch between both layers. Two regimes with different deformation modes are shown for a bilayer with a thickness of 145 nm. Adapted with permission from [40]. Copyright 2011 by the American Chemical Society. (d) A double-curved bilayer sample photographed on a reflective surface. Reproduced from [29] with permission form The Royal Society of Chemistry. (e) The curving of a star-shaped bilayer construct. Reproduced from [32] with permission from The Royal Society of Chemistry. (f) Two-step folding of a star-shaped bilayer specimen [33]. Copyright 2013 by John Wiley & Sons, Inc. Reproduced by permission of John Wiley & Sons, Inc. (g) Schematic illustration of using passive disks to control the folding angle. (h) Trilayer constructs with a heat-shrinking core. The dashed line indicates the expected folding angle as a function of the gap width. Experimental results are indicated with blue dots [61]. Reproduced by permission of IOP Publishing. (i) Trilayer samples with a swelling core. The linear dependency of the folding angle on the gap width has been verified by experiments using different thicknesses of the expanding core [63]. Copyright 2015 by John Wiley & Sons, Inc. Reproduced by permission of John Wiley & Sons, Inc.

In general, the thickness ratio has a stronger effect on the radius of curvature as compared with that of the stiffness ratio.

Timoshenko's bilayer theory is essentially a 2D model. Other parameters related to the 3D geometry of the actual structures, which are not captured by that theory, could influence the deformation characteristics. Both theoretical and experimental studies about bilayers of isotropic elastic materials show that the flat material adopts a double-curved shape for a small strain mismatch [29,40–48]. For a larger strain mismatch, the resulting shape approximates a single-curve, as the in-plane stretching required for a double-curved shape is formidably high. The high levels of required in-plane strains could be seen when one tries to wrap a plastic sheet around a sphere. Rolling in one direction therefore becomes energetically favorable for strain mismatches exceeding a certain threshold (Fig. 2c) [29,40,42–47]. This bifurcation from double-curvature to a major single curvature mode depends on both geometrical parameters (e.g. bilayer sheet dimensions [29,34,40,42,44,46] and layer thicknesses

[31,43,47]) and material properties (e.g. stiffness ratio [46,47]), which all affect the balance between stretching and bending energies. For example, a rectangular bilayer with an aspect ratio of 1 and relatively large thickness compared with its other dimensions adopts a spherical shape (Fig. 2d). Larger samples with the same thickness resulted in cylindrical shapes [29]. The rolling direction of the single curvature mode is determined by the aspect ratio (i.e. the ratio between the strip width and length) of the bilayers [40]. Unconstrained bilayer strips preferably curve along the shortest direction [40], which is in agreement with the observations reported by Guan et al. [30]. Numerical investigation of shape-shifting for different shapes of flat bilayers showed that the geometry highly influences the curvature direction as well [49]. A star-shaped polymeric bilayer produced by the deposition of a 4 μm layer of passive polymer on top of a thermo-responsive swellable polymer with equal thickness has been proposed for reversible encapsulation and release of cells (Fig. 2e) [32]. The isotropic swelling of the active layer in an aqueous environment in response to temperature changes resulted in the bending of the star arms towards each other.

Controlling the diffusion pattern of water into the swellable polymeric bilayer could be used to program the activation pattern [33,35]. A star-like bilayer of active and passive polymer produced based on the deposition of active and passive layers on top of a flat silicon substrate has been used to restrict the diffusion directions [33]. The water could only diffuse inside the active layer from the edges, which results in the deformation being dependent on the outer contour of the initially flat bilayer. Because of the small bilayer thickness (<1.5 μm), rolled tubes with small radii of curvature will form along the perimeter of the bilayer followed by bending of the arms at the intersection of adjacent tubes (Fig. 2f). In contrast to unconstrained bilayers, the edge-activation and the adhesion of the polymer to the substrate cause the bilayer to preferably curve along the longest direction [50].

Multi-material 3D printing provides additional freedom to program the printed construct through spatial arrangement of the active and passive materials. Raviv et al. printed bilayer structures with an isotropic swellable layer and a passive soft polymer layer [51,52]. In-series arrangement of bending bilayers and passive disks, which act as stoppers, has been proposed to control the level of deformation. The folding angle could then be set by changing the distance between the passive disks (Fig. 2g). An in-plane arrangement of active architected elements could then form a planar grid-like structure, which could produce curved structures upon activation. The same principle of using end-stops has been also applied in multiple trilayer structures as a technique to control the amount of deformation [53–61]. By sandwiching a shrinking layer between two structural layers, the deformation of the active layer is constrained, while small gaps in one of the structural layers allow for local bending (Fig. 2h). By applying a global stimulus, the generated stress in the active layer is locally transformed into a bending moment, resulting in bending along the folding lines. Self-folding of origami structures has been reported based on the rational patterning of hinge gaps on both structural layers of a sandwich material with a heat-shrink polymer core [59,61]. The edges of the gaps in the structural layers act as mechanical stoppers and allow for pro-

gramming the desired folding angle by adjusting the gap width [59,61]. Accurately control of folding angles up to about 120° has been reported (Fig. 2h) [61]. A swelling polymer, upon increase of humidity, has been also used as the active material to fold origami structures at microscale [62,63]. By adjusting the gap width in one of the structural layers the length of the remaining bilayer could be set resulting in a linear relation between gap width and folding angle (Fig. 2i). Folding angles ranging from 0 up to 180° have been reported [63].

Anisotropic multilayers
In order to program more complex shape transformations, one additional programming parameter could be included in the form of anisotropic material properties. By inducing stresses only in the desired direction, the deformation characteristics (e.g. the direction of rolling) could be decoupled from the geometry of the initially flat material (e.g. aspect ratio or outer contour) [64]. Self-helixing elements have been fabricated using a (mainly) uniaxial expanding/shrinking active layer for a nonzero angle φ between the main straining direction of the active layer and the main axis of the bilayer strip (Fig. 3a) [65,66]. Inspired by the opening of chiral seed pods, not only self-bending and self-helixing bilayers but also self-twisting strips could be made through combining two similar anisotropic active layers with main straining directions that are perpendicular to each other (Fig. 3b) [67–70]. Dependent on the dimensionless strip width $\tilde{w} = w\sqrt{\kappa_0/t}$, twisting or helixing will be the dominant deformation mode, where w is the strip width, t is the bilayer thickness, and κ_0 is the reference curvature (i.e. the curvature induced along the main straining direction, Fig. 3b). The twisting mode is dominated by in-plane stretching, while bending is dominant in helixing bilayers [67,69,71]. By increasing the widths of self-twisting samples, the stretching energy increases very rapidly while the bending energy of helixing constructs is only linearly related to the sample width [67,71]. Twisting is therefore energetically favorable for small widths, while self-helixing strips will be formed for $\tilde{w} \gg 1$. Based on the angle φ and the strip width w, both self-helixing and self-twisting could be programmed with different values of radius r and pitch p (Fig. 3c) [69].

Different methods have been reported for the inclusion of anisotropy within the multilayer samples. A widely reported approach is programming SMP material through uniaxial stretching. For example, multi-material 3D printing has been used to produce bilayer strips of elastomeric materials with SMP fibers embedded in one of the layers (Fig. 3d) [72,73]. The samples were stretched at high temperatures and cooled down below Tg, while maintaining the straining. The programmed stress is stored as memory inside the SMP fibers, while being retained as elastic energy in the elastomer. The release of the stress causes the elastomeric layer to recover, resulting in the bending of the strip [73]. Reheating the sample will release the frozen memory, thereby recovering the original flat shape. The active self-bending elements have been integrated with passive panels to create a self-folding box (Fig. 3d). The same research group reported 3D printing of bilayer specimens comprising two elastomeric layers and embedding SMP fibers with different Tg values [74]. The specimens revealed similar programming and recovery cycles, but shape-shifting could be activated with
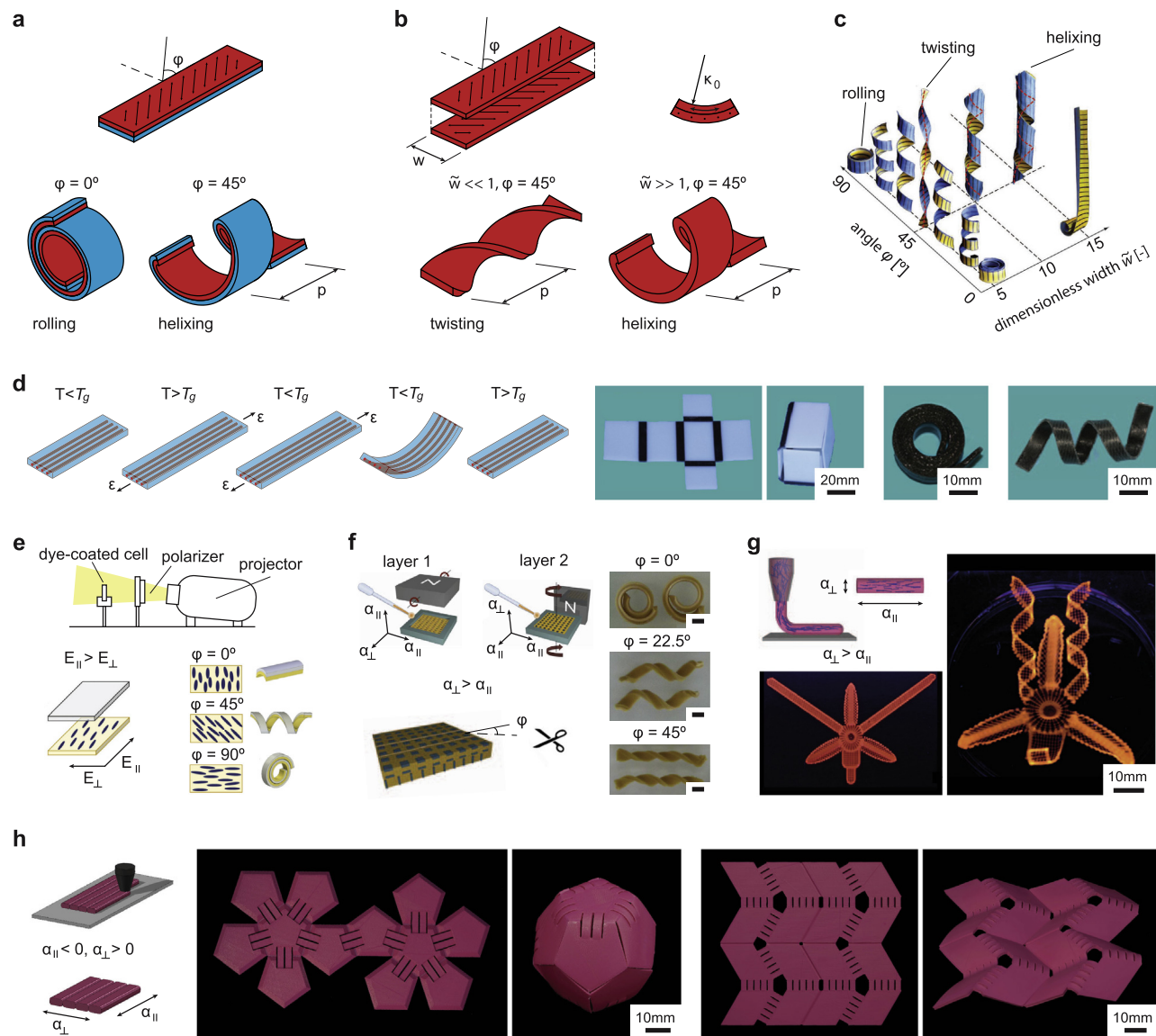
FIGURE 3

The methodology and production of anisotropic bilayers. (a) Dependency of the pitch *p* on the alignment angle ϕ. (b) Both twisting and helixing could be programmed in anisotropic bilayers. (c) The effect of alignment angle ϕ and strips width have been investigated using paper models [69]. Reproduced with permission from AAAS. (d) Programming of SMP bilayers by manually stretching of the sample has been used for different shape-shifting structures. Reproduced from [73] with the permission of AIP Publishing. (e) Spatial programming of LCE material using a digital projector. Reproduced from [79] with permission from The Royal Society of Chemistry. (f) Alignment of anisotropic platelets using a rotating magnetic field. Scale bars: 5 mm. Reproduced by permission from Macmillan Publishers Ltd: Nature Communications [68], copyright 2013. (g) Extrusion of hydrogels embedding fibrils to program anisotropic swelling. Reproduced by permission from Macmillan Publishers Ltd: Nature Materials [82], copyright 2015. (h) Simultaneous programming and fabrication of anisotropic shrinkage in SMP filament. Reproduced from [83], published by The Royal Society of Chemistry.

temperature instead of the release of the pre-strain [74]. A maximum normalized curvature of ≈ 0.75 has been realized [74]. Using both approaches, a linear relationship between the programming strain and curvature was found, while the orientation of the SMP fibers within the elastomeric strip could be changed in order to program self-helixing instead of self-rolling (Fig. 3d) [72,74]. This approach has been further extended through production of initially curved bilayers comprising two SMP layers with different *Tg* values [75]. The samples have been programmed by concurrent flattening and stretching at elevated

temperatures, thereby enabling the formation of both upward and downward curvatures upon activation. Uniaxially pre-programmed SMP material could be used as well as the active material in bilayer specimens [65]. Combined with a passive elastomeric layer, self-rolling and self-helixing have been realized by increasing the temperature. Finally, confined swelling of an isotropic hydrogel could be used for directional programming of SMP [76]. Trilayer strips have been printed using a multi-material 3D printer with a top layer of SMP, a middle layer of porous elastomeric material embedded with hydrogel, and an

elastomer bottom layer. Submersion in water results in the swelling of the hydrogel layer, while the increase in temperature reduces the stiffness of the SMP layer. Driven by the swelling of the hydrogel, the stiffness difference between the SMP and elastomer causes the specimen to curve along its shortest direction, thereby uniaxial stretching the SMP layer. After cooling and drying the sample, reheating leads to shape-recovery of the SMP layer and the strip curves back to its initial flat state [76]. As the shape-shifting is driven by the swelling of hydrogel, the process is reversible.

Uniaxial alignment of liquid crystal in a polymer network offers another strategy to introduce anisotropic mechanical properties in the active layer [10,66,77–79]. Boothby et al. used a spatially patterned photoresponsive dye coating on top of a glass slide for programming molecular orientation during the synthesis of a 30 μm thick layer of LCE material [79]. By using a digital projector of polarized light, a patterning resolution of 30×30 μm could be achieved (Fig. 3e). The LCE layer has been combined with a layer of an isotropic swellable polymer, resulting in different types of shape-shifting based on the anisotropic stiffness of the LCE upon submersion in water (Fig. 3e) [79]. Multiple shapes could be programmed in the same bilayer upon activation by high temperature, resulting in the shrinkage of the LCE layer along its molecular direction and expansion in the orthogonal direction.

Alignment of anisotropic additions in a hydrogel solution has been also reported for material reinforcement [68,80,81]. Erb et al. used a rotating magnetic field to align anisotropic platelets in a layer of hydrogel during the curing process (Fig. 3f) [68,80]. The platelets stiffen the material mostly in one direction, which

causes the hydrogel composite to show anisotropic swelling upon submersion in water. After curing, a second layer was deposited with a different anisotropy direction to create a composite bilayer [68]. This approach has been incorporated in multi-material 3D printing through different alignment of the metallic additions within each layer of liquid resin [81]. Another strategy used for localized programming of anisotropy is 3D printing of swellable polymer ink embedded with cellulose fibrils, which align in the extrusion direction [82]. The printed fibers exhibit anisotropic swelling upon submersion in water [82]. Bilayer structures have been printed, which show both self-rolling and self-twisting as well as combinations of those basic shape-shifting modes [82] (Fig. 3g). We have recently reported a new 4D printing technique capable of simultaneously fabricating and programming of SMP constructs [83]. During the process of FDM printing, directional strains (up to 40%) could be programmed inside the SMP material along the printing direction, thereby enabling programming of shape-shifting based on printing patterns. This approach has been used for printing of bilayer bending actuators as well as monolayer passive panels, which could be integrated to form origami constructs (Fig. 3h).

Material gradients
Instead of combining multiple different materials into a multi-layer construct, a gradient in the material properties of a mono-layer construct could be used to generate a stress gradient along the thickness of the material. This programming strategy offers some advantages as compared to bilayer structures. Firstly, the high shear stresses at the interface of two different materials will be avoided, thereby eliminating the risk of delamination and/or
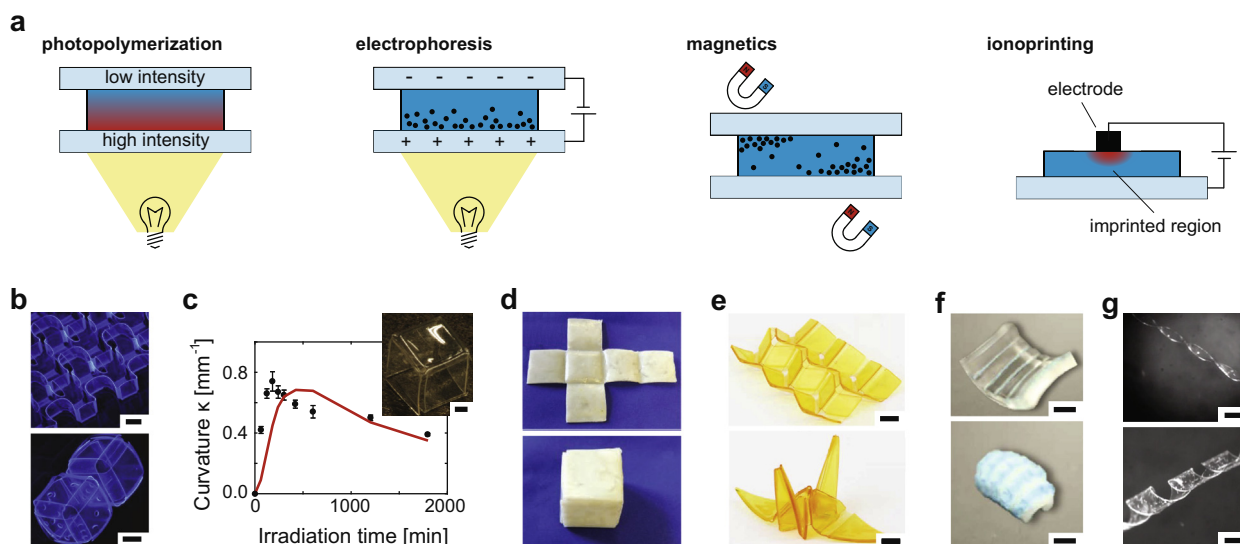

FIGURE 4

(a) Four different techniques which have been reported for production of shape-shifting materials with a through the thickness gradient in material properties. (b) Self-assembly of different origami and kirigami constructs. Scale bars: 500 μm. Reproduced by permission from Macmillan Publishers Ltd: Nature Communications [84], copyright 2011. (c) Self-folding of a cubic box. The radius of curvature could be tuned based on the irradiation time. Scale bar: 2 mm. Reproduced from [87] with the permission of AIP Publishing. (d) Self-folding of a manually programmed SMP box [89]. Copyright 2010 by John Wiley & Sons, Inc. Reproduced by permission of John Wiley & Sons, Inc. (e) Folding of complex origami constructs. Scale bars: 5 mm. Reproduced from [90]. (f) Curving of a hydrogel strip after ionoprinting. Drying of the sample results in curving in the opposite direction. Scale bars: 5 mm. Reproduced by permission from Macmillan Publishers Ltd: Nature Communications [96], copyright 2013. (g) Self-helixing and self-twisting specimens. Scale bars: 5 mm. Reproduced from [101].

interfacial sliding. Secondly, fabrication of multilayer structures often requires multiple fabrication steps, which could be reduced in the case of a single material layer.

Based on the above-mentioned programming strategy, polymerization of a photocurable polymer resin has been reported in several studies as a simple approach for production of self-rolling structures [84–86]. During the polymerization process, the light is exposed from one side while being partially absorbed by the polymer, which results in a gradient in light intensity along the material thickness (Fig. 4a). Jamal et al. used this approach to create a gradient in the crosslinking density of a layer of swellable material [84]. The stiffness of the material increases with higher crosslinking density, thereby reducing the swelling ratio of the material. Submersion in water therefore results in curving. Passive panels have been made by using high energy light exposure, giving rise to fully crosslinked materials [84,85]. Bidirectional curving has been achieved by light exposure from both the top and bottom sides. Different patterns of light exposure have been used for production of complex constructs comprising passive panels with thicknesses of about 10 μm and bidirectional folds with radii of curvature of ≈200 μm (Fig. 4b) [84]. A similar technique of using laser for partial relaxation of pre-strained polymer sheets has been used for programming stress gradients [87,88]. Semi-transparent samples were pre-strained at high temperatures (above Tg) and were exposed from one side to light to trigger stress relaxation [87]. Light absorption in the semi-transparent polymer results in a difference in light intensity at the top and bottom sides of the sample, thereby programming a different amount of stress relaxation through the thickness of the material. After programming the stress relaxation, the release of the pre-strain results in the curving of the specimen. Dependent on the irradiation duration and intensity, the desired stress gradient could be programmed, while non-irradiated passive panels are produced using a photomask (Fig. 4c) [87]. Manual programming of a single layer of SMP material has also been reported [89]. Flattening of a 3D deployable SMP sample above its Tg has been used for programming the desired stress gradient, which is stored in the material by lowering the temperature. Upon temperature increase above Tg, the desired 3D shape recovers (Fig. 4d). The concept of volume shrinkage of a photocurable polymer resin during the polymerization process has been recently reported as shape-shifting technique [90]. Based on the light intensity gradient along the thickness of material, a stress gradient could be created, which results in spontaneous curving of the structure after release from the substrate. This technique has been used for assembly of origami structures at the macroscale (Fig. 4e) [90].

A gradient in the material properties could also be generated by creating a gradient of particles along the thickness of an active material in order to locally reduce the swelling/shrinkage ratio [91–95]. Asoh et al. used electrophoresis during the photopolymerization process to program a gradient of electrically charged particles in a swellable polymer (Fig. 4a) [91]. Deswelling of the polymer, in response to increase in temperature, is inhibited by the charged particles, resulting in curving of the material [91]. Liu et al. used a magnetic field to create a gradient of magnetic nanoparticles in a swellable polymer (Fig. 4a) [92]. An increased particle concentration increases the deswelling rate while reducing the deswelling ratio, resulting in curving of the initially flat material in one direction followed by curving in the opposite direction [92]. The intensity and orientation of the applied magnetic field is used to spatially program the magnetic nanoparticles gradient, which gives local control of the curvature of the material upon deswelling.

Ionoprinting offers another strategy for programming of a bending moment in a single layer of material [96,97]. By applying a potential field, metallic ions could be embedded inside hydrogel layers. The ions will diffuse from the electrode and bond to the hydrogel network, thereby enhancing the localized crosslinking and resulting in stiffening and deswelling of the material [96,97]. Subsequent drying of the hydrogel may induce a second shape transformation as further deswelling in the imprinted region is inhibited due to the high amount of crosslinking (Fig. 4f).

A gradient in the nematic direction of liquid crystals in a polymer network could be used as well to program self-rolling and self-helixing strips in response to temperature change and humidity [98–105]. In this approach, the main straining direction (and not the amount of swelling/shrinkage) is varied over the thickness of the material. Similar to the bilayer strips with two active anisotropic layers, both self-helixing and self-twisting could be programmed dependent on the strip width and angle φ (Fig. 4g) [100,101].

Localized activation

Non-homogenous exposure of the material to the activation stimulus is another strategy to induce a stress gradient along the thickness of a monolayer material. Using this strategy, a dynamic gradient in swelling/shrinkage could be created inside the material, as the diffusion of the applied stimulus (e.g. heat or solvent) inside the material takes time. Continuous exposure to the activation stimulus will cause the diffusion to be completed, resulting in uniform swelling/shrinkage through the material thickness, thereby inhibiting out-of-plane bending.

One-sided activation of initially flat material by exposure to humidity is reported by Holmes et al. [106]. Placing a droplet of a favorable solvent at one side of a thin elastic planar material leads to the localized swelling of the material. Dependent on the viscosity of the solvent, the time at which the maximum curvature is reached has been shown to vary over two orders of magnitude (∼0.1–10 s) for a beam with a thickness of about 1 mm. Soon after activation, the normalized curvature attains its maximum value of about 0.33 which is only 22% of the theoretical limit for bilayer constructs (Fig. 5a). Similar trend of deformation is found by Reyssat et al. and a maximum curvature equal to 40% of the theoretical maximum could be achieved [107].

In contrast to humidity, light could be applied with both high spatial and temporal resolutions, thereby offering an attractive approach for accurate programming of shape-shifting [108]. Wang et al. produced a hydrogel monolayer, which at one side was embedded with nanoparticles to transform the irradiated light into heat, resulting in localized de-swelling of the hydrogel. The direction of bending was determined by the microstructure (i.e. through the thickness gradient of nanoparticle concentration), while the amount of deformation depended on the exposure time and irradiation power density [109]. A similar
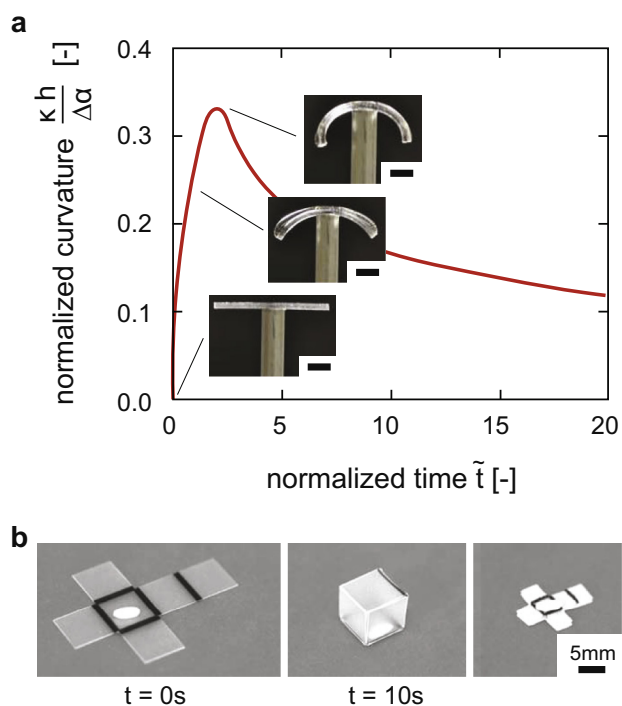
a

b

t = 0s   t = 10s

FIGURE 5

(a) Normalized curvature as a function of time, normalized by the effective diffusivity D and material thickness h as follows: $\tilde{t} = tD/h^2$. Scale bars: 3 mm. Reproduced from [106] with permission from The Royal Society of Chemistry. (b) Self-folding of a cubic box activated by exposure to infrared light. Continuous exposure results in the entire material being activated. Reproduced from [112] with permission from The Royal Society of Chemistry.

approach has been used for relaxation of 0.3 mm thick pre-strained SMP sheets, which were completely covered by black ink [110]. One-sided irradiation with laser (beam width: 500–1700 μm) locally heats the black ink, thereby heating the underlying polymer above its glass transition temperature, Tg, leading to strain recovery. Using this method, the desired shape-shifting pattern could be "written" in the material with a laser [110].

Instead of using a localized stimulus, the material sensitivity to a global activation stimulus could be programmed in the material as well [111,112]. Liu et al. patterned optically transparent sheets of pre-strained SMP with black lines, which transform the global exposure to infrared light to localized increase in the temperature (Fig. 5b) [112]. Folding angles up to 120° could be achieved by changing the width of the patterned lines, which sets the length of the curving region. By increasing the exposure time, the structure will curve back to the flat state, while exhibiting uniform shrinkage. Both sides of the transparent material could be patterned with black lines in order to program bidirectional folding, thereby creating a powerful tool for production of origami and kirigami constructs [113]. The bending direction of similar constructs could be also programmed by patterning the hinge regions with a thin structural layer covered with black ink [114]. Upon activation, shrinkage at the top side is constrained and the material will curve in the opposite direction, once the heat has diffused through the thickness of the construct [114].

An interesting direction for further research would be tuning the dynamic behavior of the constructs through spatial programming of the diffusion of activation stimuli. By programming the microstructure of material, both the diffusion rate and diffusion patterns could be set as desired.

Buckling strategy

In this approach, there is no need for through the thickness gradient in the material properties. By programming the in-plane arrangement of different active and passive elements, the desired compressive stresses could be generated upon activation. Externally generated compressive forces are used as well to induce out-of-plane buckling in a layer of passive material. Both methods have been implemented in a wide range of shape-shifting materials.

The local distances between the adjacent points on a surface are described by the metric tensor g of that sheet. By programming the in-plane dimensional changes, a target metric $\overline{g}$ is prescribed and compressive stresses could be generated. Those in-plane stresses could be relieved when the construct adopts a 3D shape, thereby minimizing its elastic energy which can be expressed as the surface integral of the elastic energy density function w (for the sake of simplicity written for the one-dimensional case):

$$w = \frac{1}{8}Et(g - \overline{g})^2 + \frac{1}{24}Et^3\kappa^2$$

where E is the material stiffness tensor, t is the material thickness, and κ is the surface curvature [24,115]. As presented in the introduction, it could be seen that the elastic energy is composed of a stretching term, which is a function of the in-plane stretching and a bending term which is related to the surface curvature. In the case of an infinitesimal thickness, the bending term is negligible and a stress-free state could be obtained when the metric tensor of the surface matches the target metric. However, such a stress-free configuration does not always exist, which results in a shape as close as possible to the target metric. By increasing the material thickness, the balance between the stretching and bending energies results in deviations from the target metric.

The buckling strategy is observed in nature as well in the form of differentially growing soft tissues [116–118]. For example, simple in-plane growth processes provide the mechanism for the shaping of leaves and other thin membranes.

Material tessellation

Instead of stacking multiple layers which exhibit different dimensional changes in response to certain stimuli, the different materials could be tessellated in a single layer construct as well. A widely-used method for production of material tessellations is the photo-polymerization of swellable hydrogels. Controlled by the amount of light exposure, the conversion of monomers and the degree of crosslinking are enhanced, thereby increasing the material stiffness. When submerged in an aqueous medium, the swelling ratio of the hydrogel is dependent on the crosslinking density. By controlling the pattern and amount of light exposure, regions with different swelling ratios could be created to generate in-plane compressive stresses upon activation.
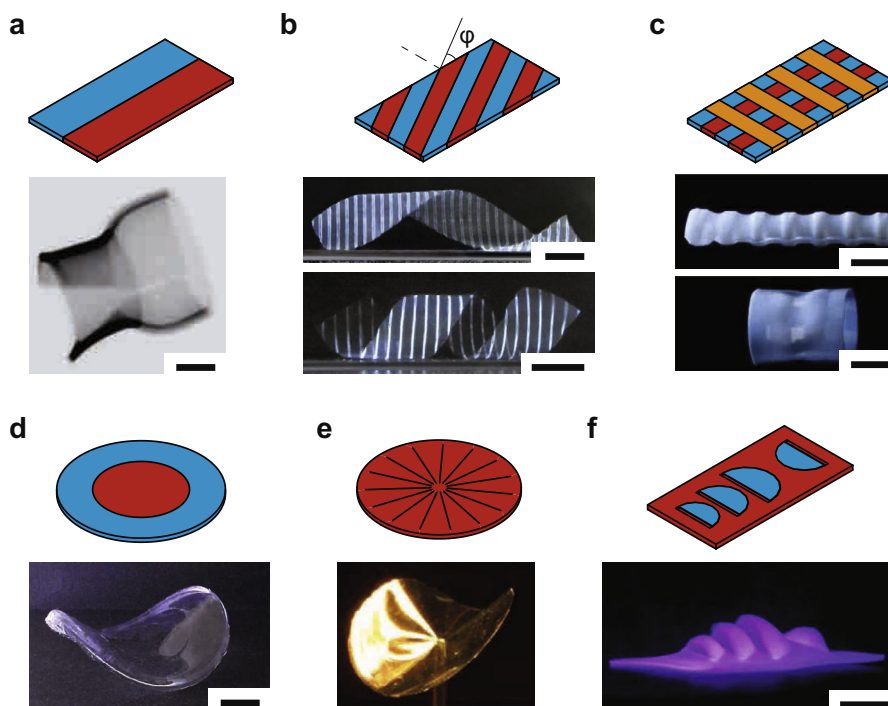
FIGURE 6

Multiple material tessellations resulting in different shape-shifting materials. (a) A bistrip of differentially swelling strips adopts a cylindrical shape upon submersion in an aqueous environment. Scale bar: 200 μm. Reproduced from [119] with permission from The Royal Society of Chemistry. (b) Parallel alignment of multiple strips could be used to program self-helixing dependent on the orientation angle ϕ. Scale bar: 1 cm. Reproduced by permission from Macmillan Publishers Ltd: Nature Communications [124], copyright 2013. (c) Programming of multiple shape transformations using different responsive materials. Scale bar: 1 cm. Reproduced with permission from [123]. Copyright 2013 by the American Chemical Society. (d) Axisymmetric material tessellations used for programming of a negative Gaussian curvature. Scale bar: 1 cm. Reproduced from [29] with permission from The Royal Society of Chemistry. (e) Alignment of a liquid crystal in a single layer of material resulting in a saddle-like shape [104]. Copyright 2012 by John Wiley & Sons, Inc. Reproduced by permission of John Wiley & Sons, Inc. (f) Incorporation of cuts in the material tessellation allows for programming more complex shapes including the Sydney opera house. Scale bar: 1 cm. From [126]. Copyright 2016 by John Wiley & Sons, Inc. Reproduced by permission of John Wiley & Sons, Inc.

One simple example of a swellable material tessellation in single layer constructs is the parallel alignment of two hydrogel strips with high and low swelling ratios (volumetric expansion of 4.3 and 2.2, respectively) [119]. Swelling in an aqueous environment results in self-rolling around the width direction of the bistrip, which allows the high-swelling strip to adopt a longer length as compared to the low-swelling strips, thereby minimizing its strain energy (Fig. 6a). The balance between the stretching and bending energies at the interface of both strips results in a transition region whose dimensions have been found to be dependent on the thickness and width of the individual strips [120,121]. Samples with parallel arrangement of multiple strips with alternating high and low swelling ratios have been prepared as well [122–124]. Dependent on the orientation of the strips with respect to the longitudinal direction of the sample, self-rolling and self-helixing elements could be created (Fig. 6b) [123,124]. This concept may be extended by producing samples with strips in both the length and width directions of the sample, which are responsive to different stimuli (e.g. temperature and pH). In this way, multiple shape transformations could be programmed in initially flat structures (Fig. 6c) [123–125]. However, this approach seems to be limited to cylindrical shapes while the minimum feature size (i.e. width of individual strips) has to be larger than about 5 times the sample thickness in order to achieve global buckling, which is a serious restriction on the

minimum sample dimensions [120]. For smaller strips, the samples remain flat, although anisotropic in-plane deformations have been observed as well. In contrast to multilayer self-rolling structures, there is a nonlinear relationship between the rolling radius on the one hand and the mismatch in swelling ratio and sample thickness on the other, resulting in a normalized curvature that is dependent both on the swelling mismatch and thickness [120]. The experimental results of Byun et al. show a maximum normalized curvature of about 0.1 for a sample thickness of 11 μm and a linear swelling mismatch of 2.0 [120]. Given the nonlinear dependence on both parameters, further reduction of the thickness and increase of swelling mismatch may result in larger values of the normalized curvature.

Axisymmetric material tessellation is another approach used for programming shape-shifting to double-curved 3D geometries into flat materials [29,126–128]. For example, a high-swelling disk surrounded by a low-swelling ring results in a dome-shaped surface upon activation, while a saddle-shaped surface could be created by interchanging the material properties of the disk and ring (Fig. 6d) [29,128]. In both cases, the maximum curvature could be achieved when the diameter of the inner disk is about 75% of the outer ring diameter [126,128]. Similar surfaces could be generated by using a disk with azimuthal alignment of liquid crystals in a polymer network [104]. Upon temperature increase, the disks shrinks in the tangential direc-

tion, while it expanding in the radial direction, resulting in a conical shape. A saddle-like shape could be created when using the radial alignment of the liquid crystals (Fig. 6e) [104].

Another study reported the use of a digital projector for 3D printing of hydrogels [126]. By programming the light exposure at every 'pixel' of a monomer solution in between two glass slices, the cross-linking density of the material was spatially controlled [126]. A large variety of double-curved surfaces could be programmed in flat hydrogels using this strategy (Fig. 6f) [126].

By patterning a single layer of material, both cylindrical and double curved shapes could be created based on the pattern of material tessellation. In most cases, hydrogels have been used as the active material in such designs, meaning that the applications are limited by the low-stiffness values and the requirement to have an aqueous environment. Moreover, the reported examples are limited to simple geometries. Given the programmed in-plane swelling/shrinkage, the 3D configuration could be predicted through minimization of the elastic energy. This forward problem has been solved for some of the presented examples [119,120,128]. However, being able to solve the inverse problem, i.e. what deformations have to be programmed for generation of a desired shape, would be required for practical applications and is a promising direction for further research.

In-plane material gradients

In contrast to the previously discussed discrete variations in the in-plane swelling/shrinkage ratios, smooth gradients in swelling/shrinkage ratios could be used for generation of stress-free 3D shapes. Sharon et al. used the injection of a solution with controllable monomer concentration into a Hele-Shaw cell to program radial gradients in the swelling ratio into a thin disk (thickness: 0.3–0.5 mm, radius: 50 mm) [129,130]. Dependent

on the programmed gradient, both wave-shaped and dome-shaped surfaces were formed upon submersion in a high temperature water bath (Fig. 7a). The axisymmetric dome-shaped configuration deviates only slightly from the desired stretch-free state as the bending energy content is limited due to the small material thickness [130]. In the case of a negative Gaussian curvature, the effect of material thickness on the final shape is more dominant as is clear from the number of wrinkles for different thicknesses. An increasing number of wrinkles corresponds to a larger bending component as well as decreased stretching energy [130]. The number of wrinkles were therefore found to be roughly proportional to $t^{-0.5}$, where t is the material thickness (Fig. 7b) [131].

Another approach is to use a gradient in the grey values of the photomask during the photo-polymerization process to program smooth gradients in the cross-linking of a swellable polymer disk [123,132]. The localized swelling ratio could also be programmed through lithography to pattern highly cross-linked dots in a swellable polymer with a low cross-link density matrix [133]. By controlling the amount of highly cross-linked dots as well as the dimensions of the dots in a certain area, the average swelling ratio could be programmed. A nearly closed spherical shape could be made by programming gradients in areal swelling ratios ranging from 2 to 8 (Fig. 7c) [133]. Potentially, arbitrarily complex shapes could be made using this technique, which is illustrated by an example comprising both regions with positive and negative Gaussian curvatures (Fig. 7c). As the buckling direction is determined by small imperfections, different surfaces could be obtained after activation for similarly programmed flat materials (Fig. 7c) [133]. Complex surfaces with non-constant Gaussian curvatures are therefore difficult to create.
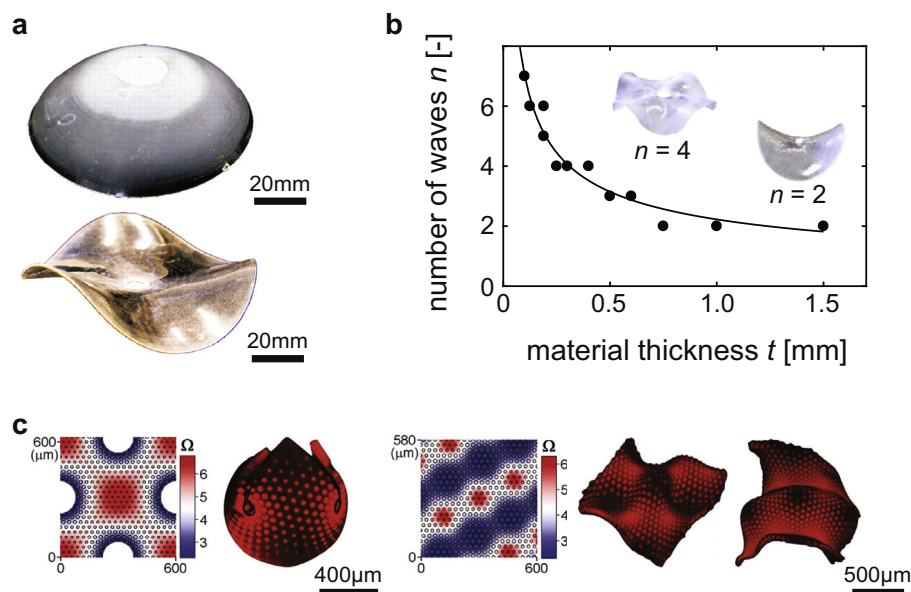

FIGURE 7

(a) A radial gradient in swelling ratio could be used for programming of both dome-shapes and saddle-shapes [130]. Reproduced with permission from AAAS. (b) Experimentally obtained dependency of the number of wrinkles on the material thickness. Reproduced with permission from [131]. Copyright 2011 by the American Physical Society. (c) Complex patterns of in-plane swelling ratios have been used for programming of a spherical shape as well as a surface comprising multiple regions with positive and negative Gaussian curvatures [133]. Reproduced with permission from AAAS.

Non-homogenous exposure

Non-homogenous exposure to the activation stimuli has been also used for programming a large variety of shape transformations. As the shape-shifting is not programmed inside the material but is based on the 'pattern of activation', many different configurations could potentially be realized within the same construct. One example is the embedding of nanoparticles inside a hydrogel sheet, which enables transformation of the illuminated light into heat, thereby promoting the deswelling of the hydrogel [134]. Complex double-curved surfaces could be programmed based on the pattern of light exposure [134]. The same approach of "light writing" for programming of shape-shifting has been used for local relaxation of pre-strained SMP through laser-assisted heating [135]. Attaching stretchable micro-electrodes to a single sheet of thermo-responsive hydrogel allows for the local control of temperature using Joule heating, thereby enabling the programming of different swelling/de-swelling ratios [136]. Multiple shape transformations may then be programmed in one structure by controlling the input power of each electrode [136].

Mechanically induced buckling

Compression of a stiff top layer by induced dimensional changes in a soft substrate is widely used to induce surface wrinkling [22,137–139]. Buckling of the thin top layer is energetically favorable over compression, causing the wrinkles to pop-up. Further compression of the bilayer could also cause delamination at the interface of both layers, resulting in buckle-delamination instead of surface wrinkling dependent on the stiffness ratio of both materials and the interfacial defects [140]. By spatially programming the adhesion between the layers, delamination occurs in a controlled manner, thereby offering a strategy for out-of-plane shape-shifting (Fig. 1b). Spontaneous delamination has been reported as well but will not be considered here [141].

Controlled out-of-plane buckling of nanoribbons was first reported by Sun et al. using a pre-strained soft substrate (thickness ≈ 4 mm) locally bonded to semiconductor nanoribbons (thickness ≈ 500 nm) [142]. Upon releasing the substrate, the thin top layer will be subjected to compressive forces, resulting in out-of-plane buckling (Fig. 8a). The semiconductor material behaves like a flexible material as the thickness of the top layer is very thin and shows a low bending stiffness. The same approach but using different top layer geometries and well-defined bonding sites is reported for production of complex 3D shapes at the mesoscale on top of a soft substrate (Fig. 8b) [143]. Additional complexity could be added in the form of spatial variations in thickness of the top layer in order to locate the folding lines, thereby allowing for programming of both origami and kirigami constructs (Fig. 8c) [144]. Another study reported the addition of multiple overlapping top layers to create more complex topologies (Fig. 8d) [145]. More details on the shape-shifting strategy of mechanically induced buckling could be found in other reviews [4,146]. An interesting future direction may be the use of different active materials as a substrate, which allows for spatial variations in the amount of compression, thereby offering the ability to program more complex 3D topologies.
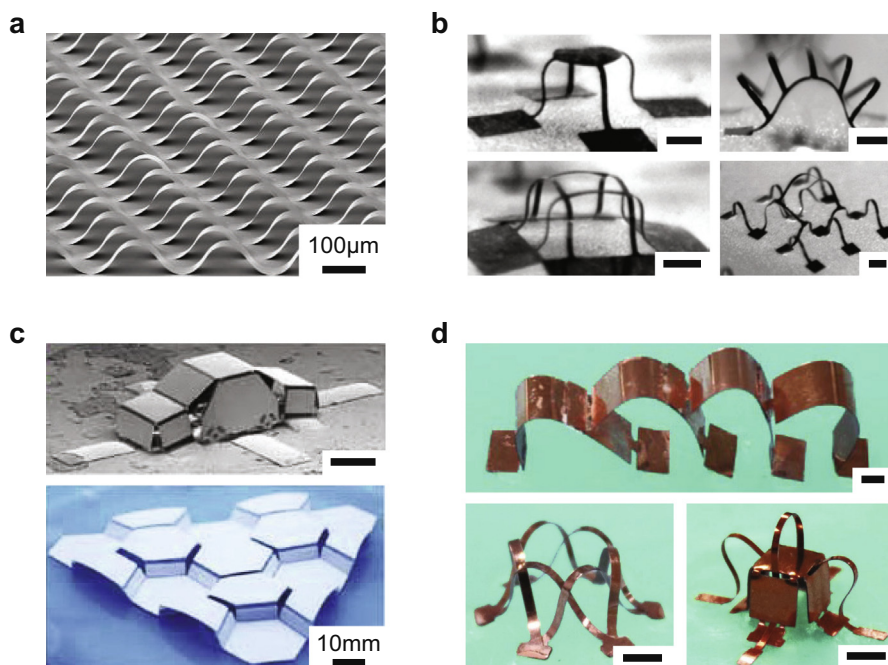
FIGURE 8

Mechanically induced buckling used for programming of different 3D constructs. (a) Thin nanoribbons on top of a thick substrate. Reproduced by permission from Macmillan Publishers Ltd: Nature Nanotechnology [142], copyright 2006. (b) Complex 3D structures at the micro-scale [143]. Scale bar: 200 μm. Reproduced with permission from AAAS. (c) Two kirigami structures made by addition of folding lines. Scale bar: 200 μm. From [144]. Copyright 2015 by John Wiley & Sons, Inc. Reproduced by permission of John Wiley & Sons, Inc. (d) Complex 3D configurations made using multiple releasable stiff top layers. Scale bar: 2 mm. Reproduced from [145].

Sequential shape-shifting

Different strategies to program 3D shapes in initially flat constructs have been discussed so far. To achieve more sophisticated shapes, it is desirable to not only program individual shape transformations but also the time sequence of the deformations. For example, this type of sequential folding could be applied in rigid panel origami to fold highly complex structures without locking the deformation by self-collisions. Moreover, appropriate locking mechanisms could be incorporated in folded structures to improve the structural/mechanical integrity of the target configuration.

Local application of the stimulus is one approach for programming the sequence of folding [54,56,135,147]. This strategy has been applied in a pre-stressed bilayer strip patterned with a stiff polymer layer which prevents curving of the construct [147]. Softening of the polymer layer upon heating by a laser allows for bending of the bilayer strip [147]. The sequence of folding

is programmed by controlling the pattern of laser light exposure. The same strategy but using Joule heating instead of laser light has been reported as well [54,56]. The hinges are activated one by one by controlling the power input at different electrodes, which allows for the self-assembly of highly complex structures.

Another strategy to program the folding sequence is to tune the material response to a time-dependent global stimulus by locally controlling the material properties [148–151]. 3D printing of origami structures with hinges made from a SMP with different T_g is reported in several studies as a tool for programming the sequence of folding [148–150]. Slowly increasing the temperature causes the hinges to start folding one by one dependent on their T_g. Both the T_g of each hinge and the time-dependent increase in the temperature are parameters that could be used to program the folding sequence. The same approach but using a swellable polymer has been reported by So et al. [151]. The temperature dependency of the thermos-responsive polymer could
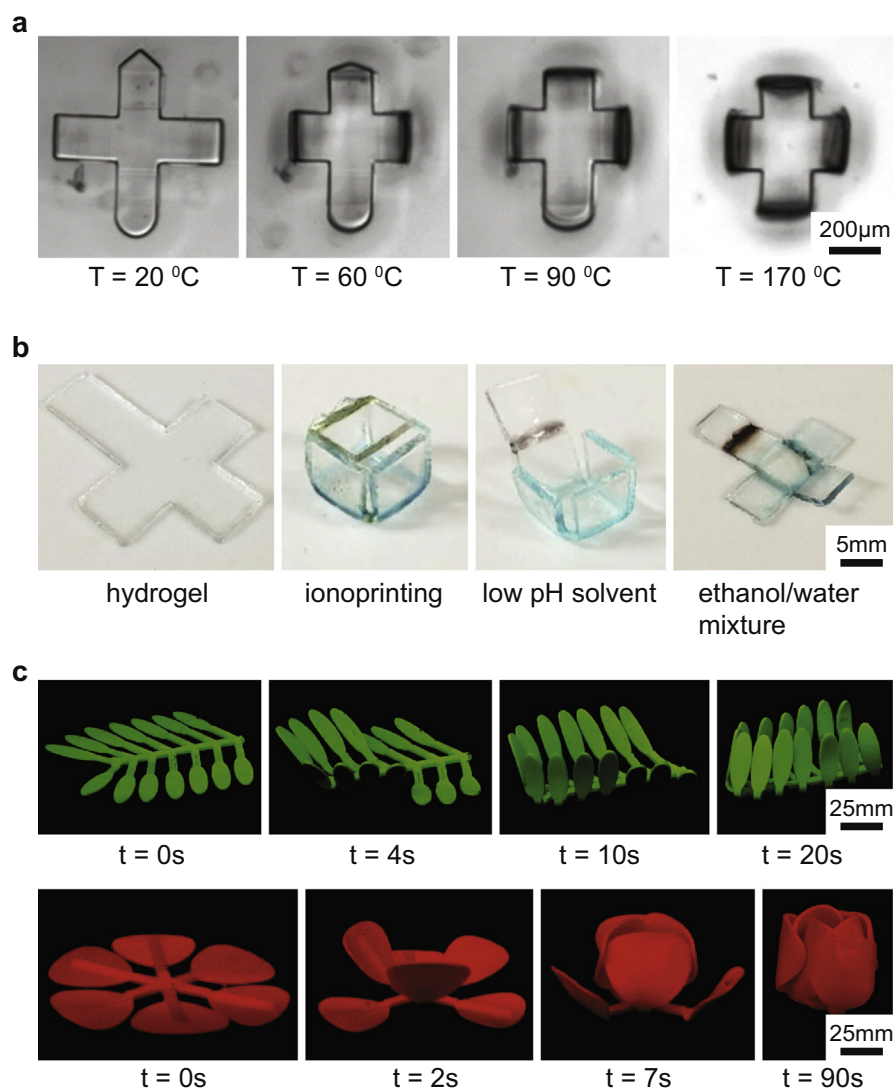

FIGURE 9

Sequential shape-shifting. (a) Sequentially closing of a box based on the environmental temperature. Reproduced with permission from [151]. Copyright 2017 by the American Chemical Society. (b) Selective unfolding of an ionoprinted hydrogel box based on the solvent. Reproduced from [152]. (c) Sequential shape-shifting based on different responses to the same activation stimulus. Reproduced from [83]. Published by The Royal Society of Chemistry.

be programmed based on the polymer composition, resulting in sequential shape transformation by a time-dependent increase or decrease in the temperature (Fig. 9a). Another variant of programming sequential (un)folding based on change in activation stimulus is ionoprinting of hydrogel using electrodes of different materials. It is then possible to imprint regions with different cations that show different deswelling behaviors based on the pH and hydrophilicity of the solvent (Fig. 9b) [152].

A third approach is to spatially program the diffusion rate of a global stimulus in the active material [83,153–155]. One study reported the patterning of lines with different grayscales at one side of a transparent pre-strained SMP sheet, which were activated by exposure to UV light [153]. Light absorption at the patterned lines leads to localized increase in the temperature. Dependent on the grayscale of the patterned lines, different amount of light energy is transformed into thermal energy thereby programming the onset time of the folding as the shape-recovery starts when the temperature approaches Tg. Because the patterned lines are applied only on one side of the material, the induced shape-recovery leads to out-of-plane curving [153]. A similar method has been reported based on using different color inks that can selectively absorb different spectrum of light which provide more freedom for controlling the process of shape-shifting [154]. Another study reported programming of the time-dependent shape-recovery of pre-strained SMP material embedded in a polymer matrix based on the interfacial area between the polymer matrix and the active material [155]. By increasing the interfacial area, the heat transfer from environment to the active SMP core could be enhanced, thereby controlling the onset time of the shape-shifting. Another method for programming the heat transfer inside SMP material is by tuning both the porosity and thickness of the 3D printed SMP bilayers [83]. The shape recovery will only commence when (almost) the whole element approaches Tg, as the stiffness of the material is much higher at low temperatures. Using this strategy, sequential folding has been incorporated into different designs (Fig. 9c).

Discussion

Two main strategies to program shape-shifting in initially flat materials were identified based on the type of internally generated stresses. Both strategies offer design routes towards generation of 3D constructs from flat soft matter but differ in their programmability options and the achievable shape transformations. Depending on the type of application and the design requirements, one of the programming strategies may be favored over another. In this section, we will discuss the benefits and difficulties of both approaches and the areas where they could be applied (as summarized in Table 1).

Programming parameters

The shape-shifting materials within the bending strategy all rely on the programming of a stress gradient along the thickness of the material. Not only the geometrical parameters and material properties but also the programming and activation conditions could be used to program the desired 3D configuration in initially flat materials. Both the bending stiffness of the structure and the induced stress gradient may be tuned to program the

desired radius of curvature of bending elements. In agreement with the Timoshenko's bilayer model, the bending curvature increases with reduced material thickness [27]. Other geometrical parameters such as the width and aspect ratio of the hinge influence the bending stiffness as well. Besides the geometrical parameters, several material properties have been changed and are shown to influence the shape-shifting. For example, the bending stiffness is influenced by the stiffness of the bulk material while the desired stress gradient is generated by the dimensional changes of the active material. The activation conditions such as the exposure time and activation energy, among other parameters are also used to program the stress gradient. In addition to the deformation amplitude (e.g. the radius of curvature) the direction of deformation (e.g. rolling or helixing) could be programmed as well. For example, the aspect ratio is shown to determine the rolling direction, if isotropic materials are used. Depending on the direction of material anisotropy, the desired pitch of a self-helixing structure could be also programmed. Finally, the shape of the target configuration may be changed by adjusting pattern of the exposure to the activation stimulus. Although the programming of bending structures has been mostly discussed within the context of multilayer constructs, these general concepts are also applicable to the other bending approaches. For example, programming parameters such as thickness or direction of anisotropy will affect the shape-shifting in a qualitatively similar way as discussed for bilayers.
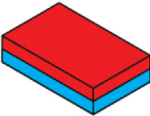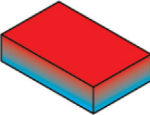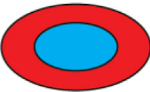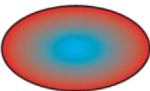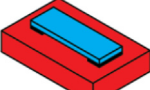
As opposed to the bending strategy, buckling is programmed through in-plane variations in swelling/shrinkage ratios, thereby generating the required compressive stresses. Based on the programmed target metric (i.e. induced in-plane dimensional changes), the structure will adopt a 3D shape by out-of-plane buckling. The buckled surface adopts a curved shape with a curvature based on the balance between the stretching and bending energies, which could be adjusted by changing the material thickness. Similar to the what was discussed for the other strategy, the activation parameters (e.g. exposure time or exposure pattern) could be used to program the in-plane compressive stress.

Programmable shapes

By inducing a stress gradient along the thickness of the material, a bending moment is generated which inherently leads to single-curved structures. Using the bending strategy, mostly developable shapes (i.e. zero Gaussian curvature) have been created as such shapes possess (almost) no stretching energy which is energetically favorable for thin constructs. Under certain conditions, such as small strain or relatively large thickness, non-cylindrical shapes could be created as well. Examples are a dome-shaped surface in case of isotropic swelling/shrinkage and self-twisting elements when the main straining direction of the anisotropic materials is varied through the thickness. As the programming strategy based on the generation of bending moment inherently results in structures with zero Gaussian curvatures, while the desired folding angle could be controlled by many different parameters, the strategy is a suitable candidate for folding of (semi-) rigid panels. Especially, trilayer constructs are often used for folding of origami structures [61,63]. It has been shown that smooth surfaces with varying curvatures could

TABLE 1

Summary of the different programming strategies.

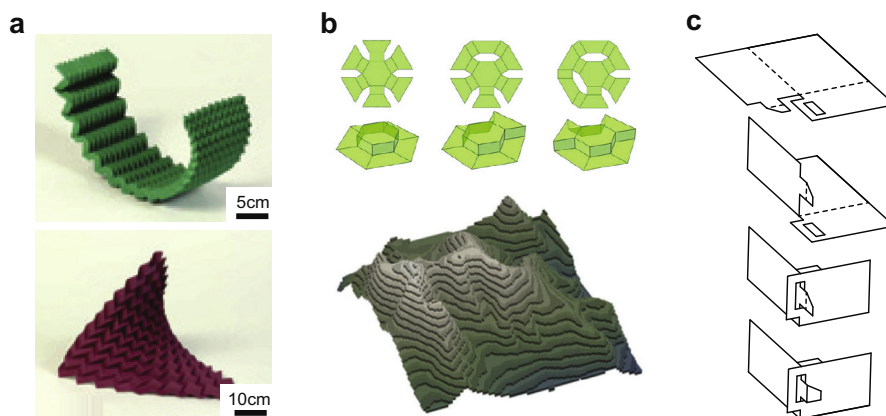|	Achievable shapes	Strategy	Advantages	Limitations	Potential applications
Bending	• Rolled shape • Helix • Twisted shape • Combinations of basic modes can create complex 3D geometries	Multilayer (Sec 2.1)	• Highest curvature • Accurate control of both direction and amount of curving based on dimensions and material properties • Versatility in selection of material	• High shear stresses at interface between layers • Multiple fabrication steps	• Folding of metamaterials [190–192,197] • Drugs delivery/cell encapsulation [168] • 3D tissue scaffolds [177] • Microgrippers [179–182] • Deployable constructs [55,185] • Sensors/actuators [18]
		Material gradients (Sec 2.2)	• Single material • No risk of delamination	• Limited curvature • Complex fabrication process	
		Localized activation (Sec 2.3)	• Single curvature • Simple fabrication • Possibility of programming multiple shapes in same material based on activation	• Limited curvature • Accurate control over activation necessary	
Buckling	• Shapes with nonzero Gaussian curvature • Local double curved shapes which show globally a developable shape	Material tessellation (Sec 3.1)	• Few fabrication steps	• High shear stresses at interface between two materials • Considerable amount of residual stresses remain after buckling • Imperfection sensitive • In-plane resolution limited to about 5–10 times the material thickness [120,133]	• Sensors/actuators [104] • Shaping of sophisticated 3D shapes [126,133]
		In-plane material gradients (Sec 3.2)	• Single material • No risk of delamination • (almost) stress-free 3D configurations possible	• Complex fabrication process • Imperfection sensitive	
		Localized activation (Sec 3.3)	• Single material • Simple fabrication • Possibility of programming multiple shapes in same material based on activation	• Accurate control over activation necessary • Imperfection sensitive	
		Mechanically induced buckling (Sec 3.4)	• Highly complex geometries can be made [143]	• Multiple fabrication steps • Structures remain connected to large substrate	• Flexible electronics [142,188,189]

FIGURE 10

(a) Approximation of smooth (double-) curved surfaces using tessellations of the Miura-ori origami. Reproduced by permission from Macmillan Publishers Ltd: Nature Materials [156], copyright 2015. (b) Kirigami elements could be used for folding of complex double-curved surfaces. Reproduced from [157]. (c) Locking elements could be implemented using sequential folding.

be approximated by folding of a flat sheet using origami tessellations (Fig. 10a) [156]. Folding of kirigami elements (i.e. voids are included in the flat material) could also be used for algorithmic design of a large range of discretized target shapes including double-curved surfaces (Fig. 10b) [157]. Other techniques based on for example curved creases or concentric pleats could also result in geometries with apparent intrinsic curvature [158]. Ornamented with a secondary level of surface nano-patterning these techniques can serve as a general platform for fabrication of functionalized metamaterials.

Compared with the bending strategy, buckling provides access to a wide range of shapes incorporating both mean and Gaussian curvature. For example, nearly developable surfaces (i.e. zero Gaussian curvature) could be created through the parallel alignment of strips with different swelling ratios, although the samples locally adopt a double-curved shape. Furthermore, simple dome-shapes and saddle-shapes have been reported, which could be generated through programming of an axisymmetric target metric. By incorporating cuts in flat materials, more complex 3D configurations have been created such as a 3D theater complex similar to the Sydney Opera House (Fig. 6f) [126]. However, as the buckling strategy is instability-driven, the direction of out-of-plane deformation is difficult to control. Because of this, (almost) no buckled constructs exhibiting multiple regions with both negative and positive Gaussian curvature have been reported. As programming the in-plane dimensional changes generally will lead to buckled surfaces with nonzero Gaussian curvature, the folding direction and folding angle could be accurately controlled using bending elements, which shows how combining both strategies could enable expanding the range of achievable target shapes.

Sequential folding has only been reported as a tool in the folding of (semi-)rigid panels. By planning the sequence of folding, the space of achievable shapes could be largely extended as self-collision between the panels may be avoided (Fig. 9c). In addition to increasing the range of achievable shapes, the integrity of the resulting (origami) structures may be improved as illustrated in Fig. 10c. Using sequentially folded collar faces, the

stability and controllability of rigid panel folding could be enhanced as well [153].

Applications

Using shape-shifting of initially flat material for the production of 3D shapes offers two promising advantages, which give rise to many new applications. First of all, shape-shifting provides access to the material surface, thereby allowing the use of 2D production techniques (Fig. 11a). Secondly, the presented techniques could be used for programming well-prescribed motions. A number of biomedical applications as well as other applications, which benefit from those advantages, will be highlighted here.

Medical applications

Multiple areas for biomedical application of shape-shifting have been identified by Randall et al. [159]. Packaging and delivery of drugs has been mentioned as one of those applications [160]. Important features of drugs delivery systems are size, shape, porosity, and surface texture, among other attributes which are necessary for accurate control of both targeting and release of drugs [161–164]. The usage of high-tech 2D production systems makes it possible to incorporate many of those features into a flat construct. Upon activation, hollow polyhedral containers could be created that incorporate those important surface features. For example, self-assembly of hollow constructs with precisely-patterned porosity is reported, which allows for a well-controlled release of drugs [165]. Self-folding devices may be applied in cell encapsulation as well [166]. Cell encapsulating systems are used to create a safe microenvironment to protect the encapsulated cells from the outside environment while acting as a platform for drugs delivery [167]. Once more, the ability to produce flat structures with highly detailed surface features using conventional 2D production techniques makes the application of self-folding devices attractive. Successful implementation of self-folding devices with the aim of cell capturing has been also reported (Fig. 11b) [168].
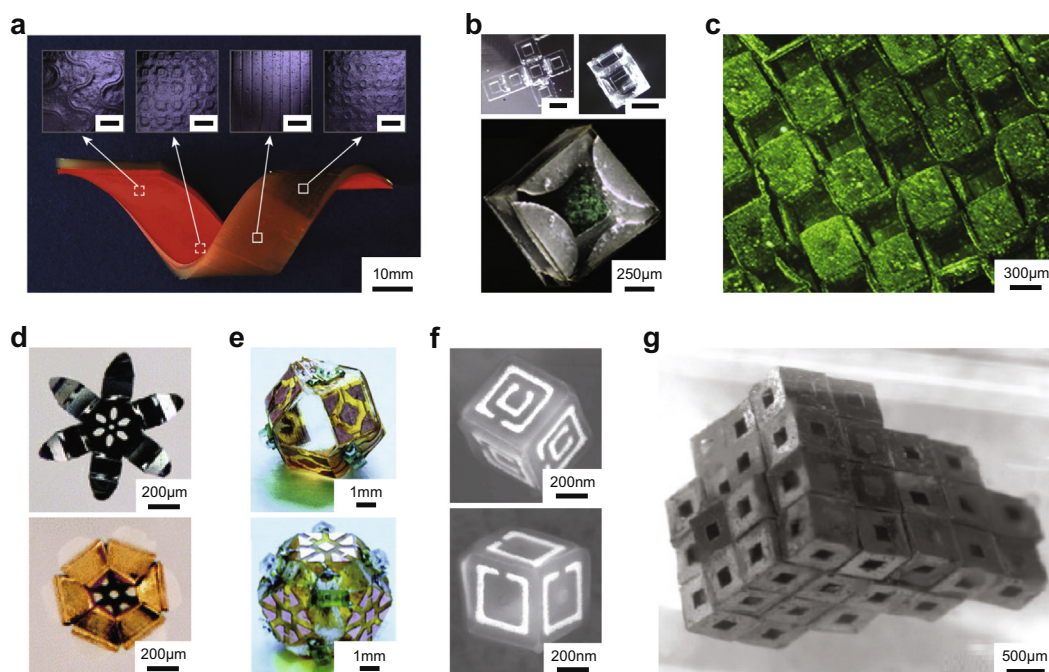
RESEARCH: Review

FIGURE 11

The potential applications of shape-shifting materials. (a) A self-helixing bilayer strip decorated with different surface patterns. Scale bars inset: 1 mm. Reproduced from [65]. Published by The Royal Society of Chemistry. (b) A self-folding box used for encapsulation of living fibroblast cells. Scale bars: 1 mm. Reproduced from [168] with permission from Springer. (c) Fibroblast cells growing on a self-folded scaffold. Reproduced from [177] with permission from Elsevier. (d) Closing of a microgripper. Reproduced with permission from [182]. Copyright 2010 by the American Chemical Society. (e) Self-folding polyhedron embedded with electric circuits [186]. Reproduced with permission from AAAS. (f) Two self-folded cubic boxes embedded with optical features [190]. Copyright 2011 by John Wiley & Sons, Inc. Reproduced by permission of John Wiley & Sons, Inc. (g) Self-assembly of multiple unit-cells. Reproduced with permission from [190]. Copyright 2010 by the American Chemical Society.

Tissue engineering has been also pointed out as a field for application of self-folding devices [159]. 3D tissue scaffolds mimic the in vivo situation the best while being able to control the formation of tissue through adjustment of the scaffold properties [169,170]. For example, mechanical properties as well as the scaffold geometry influence the differentiation of stem cells [171–173]. Cell differentiation is also facilitated by the nanotopography of the 3D scaffold [174–176]. The challenge to produce 3D scaffolds with well-controlled mechanical and geometrical properties makes shape-shifting materials an attractive alternative to other 3D production techniques. The ability to grow cells on a self-assembled 3D scaffold is reported by Jamal et al. [177,178]. By patterning different materials on top of an initially flat material, a 3D scaffold with well-controlled curvature could be created (Fig. 11c) [177].

Miniaturized medical devices are the third area of biomedical application which will be discussed here. In this application area, shape-shifting materials are utilized because of their ability to produce well-controlled and programmed motions. Production of self-folding micro-grippers as a surgical tool is reported in several studies (Fig. 11d) [179–182]. The devices could be manipulated using external magnetic fields, while different types of stimuli (e.g. thermal or chemical) may be used to activate the gripper.

Shape-shifting materials have also other applications in biotechnology such as the unfolding of a stent or wound-closure using shrinking sutures [183,184].

Other applications

Shape-shifting materials could be exploited also in many non-medical applications including sensors/actuators [18] and self-folding devices [55,185]. Two main areas of application will be discussed here, namely 3D electronics and origami-based metamaterials.

Both access to the flat surface and the ability to produce 3D shapes make shape-shifting materials attractive for production of 3D electronics [186,187]. Panels embedded with different types of circuits have been, for example, folded into the target shape to form an electrical network in 3D (Fig. 11e) [186]. Self-assembly is also used for fabrication of stretchable electronics [142,188,189]. Thin nanoscale ribbons acting as electrical connections could be created on top of a flexible substrate using out-of-plane buckling [142]. Stretching or bending of the substrate ensures that the thin electrical connection is only bent without any stretching so as to prevent any damage to the circuit. The self-folding of individual 3D electrical components (i.e. inductors and capacitors) has been also reported [59]. Similar to the case of electronics, shape-shifting could be applied in optics as well to create functionalized 3D shapes by embedding the flat panels with optical nanoscale features revealing different reflection spectra (Fig. 11f) [190].

Finally, folding of flat sheets may be used to create metamaterials with mechanical functionalities. For example, the Miura-ori pattern offers some unusual properties such as negative Poisson's ratio [191–194] while other folding patterns exhibit bi-stability

[195,196]. Metamaterials with optical functionalities could be folded and assembled from flat material as well [197]. Folding of origami structures is also used in other applications such as metamaterial absorbers [198], energy storage [199], and deformable solar cells [200].

Challenges and limitations

While bending is a well-described strategy for programming out-of-plane shape-shifting, buckling has been only recently recognized as a suitable programming strategy, which is reflected in the relatively limited number of studies using that approach. The buckling strategy is limited in the sense that only structures with nonzero Gaussian curvature could be made and that the direction of out-of-plane buckling depends on small imperfections that are difficult to control. Another limitation of buckling is that this strategy is merely reported using hydrogels as active material with only a few exceptions of using LCE [66,78,79,103,104] or SMP [83]. By using hydrogels as active material, shape-shifting could only be induced in aqueous environments [201]. Other limitations are the low mechanical properties (i.e. $E < 0.5$ MPa) of hydrogels [13] and a long activation time (up to several hours for a material thickness of 1 mm) due to the slow diffusion of water inside the material [14]. Those limitations has been tried to overcome by addition of different inclusions in the material. Examples are carbon nanotube-hydrogel hybrids for enhancement of the activation time [36], hydrogels with fiber reinforcements in order to increase the material stiffness [202,203], and the introduction of other hydrogel composites [204]. The bending strategy has been, however, reported for a larger range of active and passive materials, which could be activated in different environmental conditions using a wide range of activation stimuli. The shape-shifting performance of different bending approaches may be compared in terms of maximum achievable curvature. For bilayer samples, the two materials could be selected such that the difference in swelling/shrinkage in response to the activation stimuli is maximized. Given the materials and bilayer thickness, the layer thickness ratio may be tuned in order to optimize the curvature. Theoretically, a maximum normalized curvature of 1.5 could be obtained. Using the gradient approach, the maximum achievable curvature is restricted as only one single material could be used, thereby limiting the range of swelling/shrinkage mismatch. Furthermore, linear stress gradients generate bending moments that are only half of the bending moment generated in bilayer constructs with similar dimensions and swelling/shrinkage mismatches. The same limitations hold for the bending strategy when localized activation of responsive materials is used.

Shape-changing materials offer a powerful tool for the incorporation of sophisticated planar micro- and nano-fabrication techniques in 3D constructs. While multiple (potential) applications have been highlighted, many remaining challenges need to be overcome before widespread implementation of shape-shifting materials can be realized. First, shape-shifting techniques have been mostly used at the macro-scale, while many applications require shape-shifting structures with dimensions less than 1 mm. For example, 3D tissue engineering scaffolds with unit-cell dimensions of a few hundred micron could be used as a template for tissue regeneration or as a platform for studying the effects of geometrical cues on cell function [177]. Second, little to no complex assemblies of shape-shifting materials (e.g. structures comprising multiple unit-cells or with large variations in Gaussian curvature) have been reported yet. Despite the large library of shape-shifting techniques, the production of complex 3D origami structures comprising multiple unit-cells remains challenging. Several studies reported the possibility to program the time sequence of deformation which could tremendously increase the complexity of the possible 3D configurations. Accurate modelling tools that capture both the complex folding kinematics as well as the kinetics might be also helpful for realizing complex shape-shifting constructs. Another strategy could be the self-assembly of self-folded unit-cells, thereby eliminating the need for complex kinematics and accurate bending elements. For example, Randhawa et al. reported the self-assembly of hollow cubic unit-cells in an aqueous environment guided by the hydrophobic patterns at the outer surfaces of the cubes (Fig. 11g) [205]. Those patterns could be applied at the flat material surfaces prior to the self-folding process of the unit-cells. Because many reported shape-shifting materials require multiple and complex fabrication steps, simple manufacturing processes need to be developed to make the widespread application of those materials possible. The emerging field of so-called '4D-printing' might be a promising direction for single-step production of complex shape-shifting materials. By precisely controlling the locations of the (different) printed material(s), highly complex shape-shifting materials could be fabricated. Further development of those high resolution additive manufacturing techniques might allow for producing shape-changing materials at the micro-scale. In addition to the limited complexity of the 3D shapes achieved with shape-shifting, they rarely incorporate functionality-inducing surface features. The effects of those surface features (e.g. micro- and nano-topographies) on the shape-shifting behavior and vice versa are therefore not well understood. For example, differential shrinkage/expansion of the material might distort the applied surface patterns. All important aspects such as surface functionalities and complex shape-shifting constructs at small scales have to be integrated into one shape-changing material in order to fully exploit the promising concept of 2D to 3D shape-shifting.

Conclusion

The strategies used for programming the shape-shifting behavior could be classified as being either based on bending or buckling. Many studies have focused on generating bending moments to enable shape-shifting while out-of-plane deformation by buckling is a relatively new programming strategy. Both strategies differ mainly in the achievable target shapes. Integration of both strategies to benefit from the best of both worlds is recommended to increase the number of possible target configurations. Sequential folding could be also used for increasing the range of achievable shapes, while it could be used as a tool to improve the integrity and stability of the final shapes as well. Different applications are highlighted, which utilize the possibility of using conventional 2D techniques as well as the opportunity to create deployable structures with complex target configurations upon activation by a single scalar signal.

RESEARCH: Review

Acknowledgements

References

[1] C. Dawson, J.F. Vincent, A.-M. Rocca, Nature 390 (1997) 668.
[2] A.R. Studart, Angew. Chem. Int. Ed. 54 (2015) 3400–3416.
[3] A.G. Volkov et al., Plant Cell Environ. 33 (2010) 163–173.
[4] Y. Zhang et al., Nat. Rev. Mater. 2 (2017) 17019.
[5] A. Lendlein et al., Nature 434 (2005) 879–882.
[6] K.M. Lee et al., Adv. Funct. Mater. 21 (2011) 2913–2918.
[7] M. Ma et al., Science 339 (2013) 186–189.
[8] X. Shen et al., Nat. Chem. 5 (2013) 1035–1041.
[9] L. Brannon-Peppas, N.A. Peppas, Chem. Eng. Sci. 46 (1991) 715–722.
[10] L. Ionov, Langmuir 31 (2014) 5015–5024.
[11] A. Lendlein, V.P. Shastri, Adv. Mater. 22 (2010) 3344–3347.
[12] E.M. White et al., J. Polym. Sci. Part B: Polym. Phys. 51 (2013) 1084–1099.
[13] O. Jeon et al., Biomaterials 30 (2009) 2724–2734.
[14] S.-J. Jeon, A.W. Hauser, R.C. Hayward, Acc. Chem. Res. 50 (2017) 161–169.
[15] F. Liu, M.W. Urban, Prog. Polym. Sci. 35 (2010) 3–23.
[16] C. De las Heras Alarcón, S. Pennadam, C. Alexander, Chem. Soc. Rev. 34 (2005) 276–285.
[17] S.J. Woltman, G.D. Jay, G.P. Crawford, Nat. Mater. 6 (2007) 929–938.
[18] C. Ohm, M. Brehmer, R. Zentel, Adv. Mater. 22 (2010) 3366–3387.
[19] Q. Zhao, H.J. Qi, T. Xie, Prog. Polym. Sci. 49 (2015) 79–120.
[20] A. Lendlein, R. Langer, Science 296 (2002) 1673–1676.
[21] D. Ratna, J. Karger-Kocsis, J. Mater. Sci. 43 (2008) 254–269.
[22] Y. Liu, J. Genzer, M.D. Dickey, Prog. Polym. Sci. 52 (2016) 79–106.
[23] E. Efrati, E. Sharon, R. Kupferman, Soft Matter 9 (2013) 8187–8197.
[24] E. Efrati, E. Sharon, R. Kupferman, J. Mech. Phys. Solids 57 (2009) 762–775.
[25] E. Sharon, E. Efrati, Soft Matter 6 (2010) 5693–5704.
[26] P. Cendula et al., Phys. Rev. B 79 (2009) 085429.
[27] S. Timoshenko, JOSA 11 (1925) 233–255.
[28] N. Bassik et al., Polymer 51 (2010) 6093–6098.
[29] A. Egunov, J. Korvink, V. Luchnikov, Soft Matter 12 (2016) 45–52.
[30] J. Guan et al., J. Phys. Chem. B 109 (2005) 23134–23137.
[31] Z. Hu, X. Zhang, Y. Li, Science 269 (1995) 525.
[32] G. Stoychev, N. Puretskiy, L. Ionov, Soft Matter 7 (2011) 3277–3279.
[33] G. Stoychev, S. Turcaud, J.W. Dunlop, L. Ionov, Adv. Funct. Mater. 23 (2013) 2295–2300.
[34] J. Kim et al., Chem. Eng. J. 321 (2017) 384–393.
[35] G. Stoychev et al., Adv. Funct. Mater. 26 (2016) 7733–7739.
[36] X. Zhang et al., Nano Lett. 11 (2011) 3239–3244.
[37] M.S. Oh et al., ACS Appl. Mater. Interfaces 8 (2016) 8782–8788.
[38] S. Naficy et al., Macromol. Mater. Eng. 302 (2017).
[39] W. Guo, M. Li, J. Zhou, Smart Mater. Struct. 22 (2013) 115028.
[40] S. Alben, B. Balakrisnan, E. Smela, Nano Lett. 11 (2011) 2280–2285.
[41] Z. Chen et al., Phys. Rev. Lett. 109 (2012) 114302.
[42] M. Finot, S. Suresh, J. Mech. Phys. Solids 44 (1996) 683–721.
[43] E. Mansfield, Proc. R. Soc. Lond. A Math. Phys. Eng. Sci. R. Soc. (1962) 316–327.
[44] M.L. Dunn, Y. Zhang, V.M. Bright, J. Microelectromech. Syst. 11 (2002) 372–384.
[45] L. Freund, J. Mech. Phys. Solids 48 (2000) 1159–1174.
[46] B.D. Harper, W. Chih-Ping, Int. J. Solids Struct. 26 (1990) 511–525.
[47] N. Salamon, C.B. Masters, Int. J. Solids Struct. 32 (1995) 473–481.
[48] S. Lin et al., Soft Matter 12 (2016) 9797–9802.
[49] S. Alben, Adv. Comput. Math. 41 (2015) 1–22.
[50] G. Stoychev et al., ACS Nano 6 (2012) 3925–3934.
[51] D. Raviv et al., Sci. Rep. 4 (2014) 7422.
[52] S. Tibbits, Architect. Design 84 (2014) 116–121.
[53] B. An, et al., Robotics and Automation (ICRA), 2014 IEEE International Conference on: IEEE, 2014, p. 1466–73.
[54] S. Felton et al., J. Micromech. Microeng. 25 (2015) 085004.
[55] S. Felton et al., Science 345 (2014) 644–646.
[56] S.M. Felton et al., Soft Matter 9 (2013) 7688–7694.
[57] S. Miyashita, et al., Robotics and Automation (ICRA), 2015 IEEE International Conference on: IEEE, 2015, p. 1490–6.
[58] S. Miyashita, et al., Robotics and Automation (ICRA), 2014 IEEE International Conference on: IEEE, 2014, p. 1446–53.
[59] S. Miyashita et al., Smart Mater. Struct. 23 (2014) 094005.
[60] S. Miyashita, C.D. Onal, D. Rus, Intelligent Robots and Systems (IROS), 2013 IEEE/RSJ International Conference on: IEEE, 2013, p. 4065–71.
[61] M.T. Tolley et al., Smart Mater. Struct. 23 (2014) 094006.
[62] N. An, M. Li, J. Zhou, Smart Mater. Struct. 25 (11L) (2016) T02.
[63] J.H. Na et al., Adv. Mater. 27 (2015) 79–85.
[64] Z. Chen et al., Phys. Rev. Appl. 5 (2016) 017001.
[65] S. Janbaz, R. Hedayati, A. Zadpoor, Mater. Horizons 3 (2016) 536–547.
[66] L.T. de Haan et al., J. Am. Chem. Soc. 136 (2014) 10585–10588.
[67] S. Armon et al., Science 333 (2011) 1726–1730.
[68] R.M. Erb et al., Nat. Commun. 4 (2013) 1712.
[69] Y. Forterre, J. Dumais, Science 333 (2011) 1715–1716.
[70] Q. Guo et al., Appl. Phys. Lett. 104 (2014) 211901.
[71] S. Armon et al., Soft Matter 10 (2014) 2733–2740.
[72] Q. Ge et al., Smart Mater. Struct. 23 (2014) 094007.
[73] Q. Ge, H.J. Qi, M.L. Dunn, Appl. Phys. Lett. 103 (2013) 131901.
[74] J. Wu et al., Sci. Rep. 6 (2016).
[75] S. Chen et al., Appl. Phys. Lett. 110 (2017) 133506.
[76] Y. Mao et al., Sci. Rep. 6 (2016) 24761.
[77] J. Zhou, S.S. Sheiko, J. Polym. Sci. Part B: Polym. Phys. 54 (2016) 1365–1380.
[78] A. Agrawal et al., Soft Matter 10 (2014) 1411–1415.
[79] J.M. Boothby, T.H. Ware, Soft Matter 13 (2017) 4349–4356.
[80] R.M. Erb et al., Science 335 (2012) 199–204.
[81] D. Kokkinis, M. Schaffner, A.R. Studart, Nat. Commun. 6 (2015).
[82] A.S. Gladman et al., Nat. Mater. 15 (2016) 413–418.
[83] T. van Manen, S. Janbaz, A.A. Zadpoor, Mater. Horizons (2017).
[84] M. Jamal, A.M. Zarafshar, D.H. Gracias, Nat. Commun. 2 (2011) 527.
[85] C. Yoon et al., Smart Mater. Struct. 23 (2014) 094008.
[86] Z. Zhao et al., Macromol. Rapid Commun. 38 (2017) 1600625.
[87] J. Ryu et al., Appl. Phys. Lett. 100 (2012) 161908.
[88] C. Danielson et al., Soft Matter 13 (2017) 4224–4230.
[89] M. Behl, M.Y. Razzaq, A. Lendlein, Adv. Mater. 22 (2010) 3388–3410.
[90] Z. Zhao et al., Sci. Adv. 3 (2017) e1602326.
[91] Asoh Ta et al., Adv. Mater. 20 (2008) 2080–2083.
[92] Y. Liu et al., Soft Matter 8 (2012) 3295–3299.
[93] D. Morales et al., Small 12 (2016) 2283–2290.
[94] I.Y. Konotop et al., Soft Matter 6 (2010) 1632–1634.
[95] H. Tokuyama, M. Sasaki, S. Sakohara, Colloids Surf., A 273 (2006) 70–74.
[96] E. Palleau et al., Nat. Commun. 4 (2013) 2257.
[97] B.P. Lee, S. Konst, Adv. Mater. 26 (2014) 3415–3419.
[98] K.D. Harris, C.W. Bastiaansen, D.J. Broer, Macromol. Rapid Commun. 27 (2006) 1323–1329.
[99] S. Iamsaard et al., Nat. Chem. 6 (2014) 229–235.
[100] Y. Sawa et al., Phys. Rev. E 88 (2013) 022502.
[101] Y. Sawa et al., Proc. Natl. Acad. Sci. 108 (2011) 6364–6368.
[102] G.N. Mol et al., Adv. Funct. Mater. 15 (2005) 1155–1159.
[103] L.T. de Haan et al., Adv. Funct. Mater. 24 (2014) 1251–1258.
[104] L.T. de Haan, Angew. Chem. Int. Ed. 51 (2012) 12469–12472.
[105] D.-W. Lee, J. Phadikar, M.R. Shankar, RSC Adv. 7 (2017) 23046–23054.
[106] D.P. Holmes et al., Soft Matter 7 (2011) 5188–5193.
[107] E. Reyssat, L. Mahadevan, EPL (Europhysics Letters) 93 (2011) 54001.
[108] I. Tomatsu, K. Peng, A. Kros, Adv. Drug Deliv. Rev. 63 (2011) 1257–1266.
[109] E. Wang, M.S. Desai, S.-W. Lee, Nano Lett. 13 (2013) 2826–2830.
[110] Y. Liu et al., J. Appl. Phys. 115 (2014) 204911.
[111] D. Davis et al., RSC Adv. 5 (2015) 89254–89261.
[112] Y. Liu et al., Soft Matter 8 (2012) 1764–1769.
[113] Q. Zhang et al., Extreme Mech. Lett. 11 (2017) 111–120.
[114] J. Cui et al., Soft Matter 13 (2017) 3863–3870.
[115] E. Efrati, E. Sharon, R. Kupferman, Phys. Rev. E 80 (2009) 016602.
[116] H. Liang, L. Mahadevan, Proc. Natl. Acad. Sci. 108 (2011) 5516–5521.
[117] J. Dervaux, M.B. Amar, Phys. Rev. Lett. 101 (2008) 068101.
[118] S. Eran, M. Marder, H.L. Swinney, Am. Sci. 92 (2004) 254.
[119] J. Kim et al., Soft Matter 8 (2012) 2375–2381.
[120] M. Byun, C.D. Santangelo, R.C. Hayward, Soft Matter 9 (2013) 8264–8273.
[121] M. Moshe, E. Sharon, R. Kupferman, Nonlinearity 26 (2013) 3247.
[122] J. Bae et al., Polymer 55 (2014) 5908–5914.
[123] H.l. Théri.-Aubin et al., J. Am. Chem. Soc. 135 (2013) 4834–4839.
[124] Z.L. Wu et al., Nat. Commun. 4 (2013) 1586.
[125] H. Thérien-Aubin et al., Soft Matter 11 (2015) 4600–4605.
[126] L. Huang et al., Adv. Mater. 29 (2017).
[127] K.N. Long et al., Int. J. Solids Struct. 48 (2011) 2089–2101.
[128] M. Pezzulla et al., Soft Matter 11 (2015) 5812–5820.
[129] E. Efrati et al., Phys. D 235 (2007) 29–32.

[130] Y. Klein, E. Efrati, E. Sharon, Science 315 (2007) 1116–1120.
[131] Y. Klein, S. Venkataramani, E. Sharon, Phys. Rev. Lett. 106 (2011) 118303.
[132] J.-H. Na et al., Soft Matter 12 (2016) 4985–4990.
[133] J. Kim et al., Science 335 (2012) 1201–1205.
[134] A.W. Hauser et al., Angew. Chem. Int. Ed. 54 (2015) 5434–5437.
[135] T. Chen et al., Mater. Horizons 3 (2016) 581–587.
[136] C. Yu et al., Adv. Mater. 25 (2013) 1541–1546.
[137] D. Chen et al., J. Polym. Sci., Part B: Polym. Phys. 52 (2014) 1441–1461.
[138] J. Rodríguez-Hernández, Prog. Polym. Sci. 42 (2015) 1–41.
[139] S. Yang, K. Khare, P.C. Lin, Adv. Funct. Mater. 20 (2010) 2550–2564.
[140] H. Mei et al., Appl. Phys. Lett. 90 (2007) 151902.
[141] D. Vella et al., Proc. Natl. Acad. Sci. 106 (2009) 10901–10906.
[142] Y. Sun et al., Nat. Nanotechnol. 1 (2006) 201–207.
[143] S. Xu et al., Science 347 (2015) 154–159.
[144] Z. Yan et al., Adv. Funct. Mater. 26 (2016) 2629–2639.
[145] Z. Yan et al., Sci. Adv. 2 (2016) e1601014.
[146] Z. Yan et al., Extreme Mech. Lett. 11 (2017) 96–104.
[147] K.E. Laflin et al., Appl. Phys. Lett. 101 (2012) 131901.
[148] Q. Ge et al., Sci. Rep. 6 (2016) 31110.
[149] Y. Mao et al., Sci. Rep. 5 (2015) 13616.
[150] K. Yu et al., Proc. IUTAM 12 (2015) 193–203.
[151] S. So, R.C. Hayward, ACS Appl. Mater. Interfaces 9 (2017) 15785–15790.
[152] A.B. Baker, D.F. Wass, R.S. Trask, Smart Mater. Struct. 25 (2016) 10LT02.
[153] Y. Lee et al., Sci. Rep. 5 (2015) 16544.
[154] Y. Liu et al., Sci. Adv. 3 (2017) e1602417.
[155] M.Y. Razzaq et al., Adv. Mater. 25 (2013) 5514–5518.
[156] L.H. Dudte et al., Nat. Mater. 15 (2016) 583–588.
[157] D.M. Sussman et al., Proc. Natl. Acad. Sci. 112 (2015) 7449–7453.
[158] S.J.P. Callens, A.A. Zadpoor, Mater. Today (2017), https://doi.org/10.1016/j.mattod.2017.10.004.
[159] C.L. Randall, E. Gultepe, D.H. Gracias, Trends Biotechnol. 30 (2012) 138–146.
[160] R. Fernandes, D.H. Gracias, Adv. Drug Deliv. Rev. 64 (2012) 1579–1589.
[161] J.A. Champion, Y.K. Katare, S. Mitragotri, J. Control. Release 121 (2007) 3–9.
[162] S.E. Gratton et al., Proc. Natl. Acad. Sci. 105 (2008) 11613–11618.
[163] C. He et al., Biomaterials 31 (2010) 3657–3666.
[164] K.Y. Win, S.-S. Feng, Biomaterials 26 (2005) 2713–2722.
[165] Y.V. Kalinin, J.S. Randhawa, D.H. Gracias, Angew. Chem. Int. Ed. 50 (2011) 2549–2553.
[166] C.L. Randall et al., Nanomed. Nanotechnol. Biol. Med. 7 (2011) 686–689.
[167] G. Orive et al., Adv. Drug Deliv. Rev. 67 (2014) 3–14.

[168] A. Azam, K.E. Laflin, M. Jamal, et al., Biomed. Microdevices 13 (2011) 51–58.
[169] E. Cukierman et al., Science 294 (2001) 1708–1712.
[170] M.W. Tibbitt, K.S. Anseth, Biotechnol. Bioeng. 103 (2009) 655–663.
[171] A.J. Engler et al., Cell 126 (2006) 677–689.
[172] F. Guilak et al., Cell Stem Cell 5 (2009) 17–26.
[173] R.J. Pelham, Y.-L. Wang, Proc. Natl. Acad. Sci. 94 (1997) 13661–13665.
[174] L.E. McNamara et al., J. Tissue Eng. 1 (2010) 120623.
[175] E.K. Yim, S.W. Pang, K.W. Leong, Exp. Cell Res. 313 (2007) 1820–1829.
[176] S. Dobbenga, L.E. Fratila-Apachitei, A.A. Zadpoor, Acta Biomater. 46 (2016) 3–14.
[177] M. Jamal et al., Biomaterials 31 (2010) 1683–1690.
[178] M. Jamal et al., Adv. Healthcare Mater. 2 (2013) 1142–1150.
[179] J.C. Breger et al., ACS Appl. Mater. Interfaces 7 (2015) 3398–3405.
[180] E. Gultepe et al., Adv. Mater. 25 (2013) 514–519.
[181] T.G. Leong et al., Proc. Natl. Acad. Sci. 106 (2009) 703–708.
[182] N. Bassik et al., J. Am. Chem. Soc. 132 (2010) 16314–16317.
[183] K. Kuribayashi et al., Mater. Sci. Eng. A 419 (2006) 131–137.
[184] I. Ward Small et al., J. Mater. Chem. 20 (2010) 3356–3366.
[185] J. Mu et al., Sci. Adv. 1 (2015) e1500533.
[186] D.H. Gracias et al., Science 289 (2000) 1170–1172.
[187] S. Pandey et al., Micromachines 7 (2016) 78.
[188] J.A. Rogers, T. Someya, Y. Huang, Science 327 (2010) 1603–1607.
[189] Y. Zhang, Y. Huang, J.A. Rogers, Curr. Opin. Solid State Mater. Sci. 19 (2015) 190–199.
[190] J.H. Cho et al., Small 7 (2011) 1943–1948.
[191] M. Schenk, S.D. Guest, Proc. Natl. Acad. Sci. 110 (2013) 3276–3281.
[192] C. Lv et al., Sci. Rep. 4 (2014) 5979.
[193] H.M. Kolken, A. Zadpoor, RSC Adv. 7 (2017) 5111–5129.
[194] A.A. Zadpoor, Mater. Horizons 3 (2016) 371–381.
[195] B.H. Hanna et al., Smart Mater. Struct. 23 (2014) 094009.
[196] J.L. Silverberg et al., Nat. Mater. 14 (2015) 389–393.
[197] J.S. Randhawa et al., Appl. Phys. Lett. 96 (2010) 191108.
[198] Y. Shen et al., J. Phys. D Appl. Phys. 48 (2015) 445008.
[199] Z. Song et al., Nat. Commun. 5 (2014) 3140.
[200] R. Tang et al., Appl. Phys. Lett. 104 (2014) 083501.
[201] S.-K. Ahn, Soft Matter 4 (2008) 1151–1157.
[202] S. Lin et al., Soft Matter 10 (2014) 7519–7527.
[203] S.E. Bakarich et al., ACS Appl. Mater. Interfaces 6 (2014) 15998–16006.
[204] J. Chen, K. Park, J. Control. Release 65 (2000) 73–82.
[205] J.S. Randhawa et al., Langmuir 26 (2010) 12534–12539.